JOURNAL OF GEOPHYSICAL RESEARCH, VOL. 92, NO. C2, PAGES 1655–1681, FEBRUARY 15, 1987

Mesoscale Surveys Over the Shelf and Slope in the Upwelling Region Near Point Arena, California

ADRIANA HUYER AND P. MICHAEL KOSRO

College of Oceanography, Oregon State University, Corvallis

Repeated mesoscale surveys of a 40-km-wide, 100-km-long, coastal region near Point Arena, California, were conducted during the upwelling season (April–August) in 1981 and 1982. Each survey included conventional conductivity-temperature-depth casts at standard locations over the continental shelf and slope between 38°N and 39°10'N, and continuous operation of a Doppler acoustic log to obtain velocity profiles in the 20- to 150-m depth range. "Synoptic" surveys covered the entire grid in 2–3 days. Winds were strongly favorable for upwelling during the three 1981 surveys and were weak or variable during the three 1982 surveys. Surface temperature and salinity fields reflect the influence of both the seasonal winds and day-to-day variations in the wind. Persistently low surface salinities offshore reflect the general southward advection of subarctic waters, and sporadic low salinities over the inner shelf reflect northward advection of local runoff through an intermittent narrow countercurrent along the coast. Circulation patterns during all but one of the surveys were very complex and included meandering equatorward flow, cyclonic and anticyclonic eddies, and inshore countercurrents. The simple two-dimensional, equatorward, baroclinic coastal jet usually associated with coastal upwelling was observed during only one of our surveys. Overall average fields are relatively simple. They show broad equatorward surface flow, a very weak inshore countercurrent, and a definite poleward undercurrent at the shelf break. Average temperature, salinity, and density fields are generally congruent with the average flow pattern. Average isotherms and isohalines are not strictly parallel to the coastline: south of the coastline bend at Point Arena, they diverge gradually from the coast. Comparison of average sections calculated from 10 matched pairs of Central and Arena lines (separated by 50 km) shows there are systematic differences between them. Warmer, fresher waters lie nearer shore (and in shallower water) off Point Arena than on the Central line; this suggests that the surface waters flowing past Point Arena have sufficient southward momentum to cross isobaths. Comparison of average velocity sections on these two lines shows some differences in structure; since the variability is large, these may not be significant. Comparison of the measured and geostrophic average shears suggests there is a significant ageostrophic component in the upper layers above 40 m; it may be the signature of an average wind-driven Ekman spiral.

1. INTRODUCTION

As part of the Coastal Ocean Dynamics Experiment (CODE) we conducted repeated mesoscale surveys of waters over the continental shelf and upper slope in a small region off northern California to study the spatial structure of the temperature, salinity, density, and velocity fields during the upwelling season. CODE was situated between Point Arena and Point Reyes on the northern California coast (Figure 1), in a region with very strong, persistent upwelling-favorable winds and moderate variations in shelf topography. There is a definite bend in both the coastline and the shelf edge at Point Arena: isobaths have a generally north-south orientation north of Point Arena and a predominantly northwest-southeast orientation between Point Arena and Point Reyes. The shelf width is roughly uniform immediately north of Point Arena, but it gradually increases from about 15 km at Point Arena to about 30 km off Bodega Head, 90 km to the southeast.

Our survey region extends along the coast from about 20 km north of Point Arena to about 70 km south of it (Figure 1). Each survey consisted of four or five sections spanning the continental shelf and upper slope; sections were chosen to be locally perpendicular to the shelf isobaths, and each section extended about 45 km from the coast. Each section included conventional conductivity-temperature-depth (CTD) casts to a maximum depth of 1000 m and continuous operation of a Doppler acoustic log (DAL) to obtain velocity profiles to a depth of 150 m. Additional DAL velocity data were obtained during drifter deployments, runs between CTD sections, etc.

Our surveys had several purposes: to determine the general structure of the temperature, salinity, density, and velocity fields; to determine whether this general structure was persistent or highly variable; to search for relationships among thsese fields; and to determine whether there was significant alongshore variations that might be associated with the bend in the coastline or the isobath divergence. Elsewhere in this volume, *Kosro* [this issue] describes outstanding features of the DAL velocity field and their relation to the larger sea surface temperature field as seen in satellite infrared images and shows examples of vertical sections through these features. He also describes and discusses the vertical structure of the onshore and alongshore components of the average DAL velocity field. In this paper we emphasize the horizontal structure. Results are presented in three main sections. In the first we compare horizontal distributions observed during six separate synoptic surveys, using maps of shipboard winds, near-surface temperature and salinity, and DAL current vectors at three different depths. In the second we describe the general structure of the average fields, showing maps at selected depths for both measured and calculated parameters. In the third section, we compare averages of 10 matched pairs of Central and Arena lines, 50 km apart, and show that there are systematic differences between them.

Paper number 6C0386.
0148-0227/87/006C-0386$05.00

2. THE OBSERVATIONS

The mesoscale surveys were conducted during the upwelling season on three hydrographic cruises within each of the two

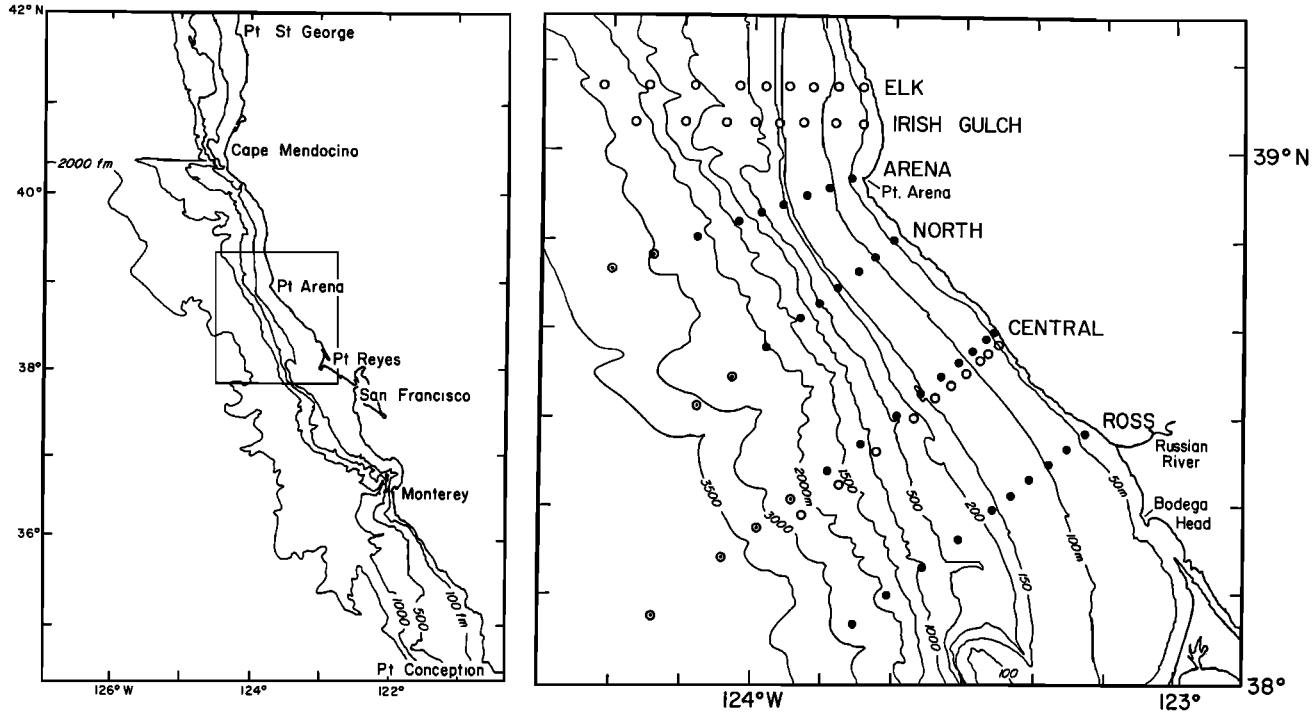

Fig. 1. Location of CTD stations and sections of the standard CODE mesoscale grid. Solid dots denote stations occupied during all of the mesoscale surveys. Open circles indicate stations occupied in either 1981 (the Elk Creek line) or 1982 (Irish Gulch and displaced Central lines). Circles with small dots were stations occupied during most (but not all) mesoscale surveys.

intensive CODE experiments: legs 4, 5, and 7 of CODE 1 (April 25 to May 7, May 16–29, and July 1–4 1981), and legs 6, 8, and 9 of CODE 2 (April 19–24, May 28 to June 4, and July 13–27, 1982). All of these cruises included CTD casts at standard locations and continuous velocity profile measurements. The survey grid (Figure 1) was designed to be large enough to cover a substantial stretch of coastline (about 100 km), and small enough to be completed in 2–3 days, a period considerably less than the typical duration (7–10 days) of strong wind-driven upwelling events. In this sense, each of the mesoscale surveys is "synoptic," or at least quasi-synoptic.

The basic design of the survey grid (Figure 1) was influenced by previous studies of other upwelling regions, which showed that alongshore gradients were generally much weaker than onshore-offshore gradients [e.g., *Brink*, 1983; *Brink et al.*, 1983], that the alongshore component of the current was generally much stronger than the onshore-offshore component [*Kundu and Allen*, 1976; *Smith*, 1981], and that the circulation pattern tended to be two dimensional, especially during strong upwelling-favorable winds [*Halpern*, 1976; *Smith*, 1981]. Accordingly, the alongshore spacing between sections is much larger (20–30 km) than the onshore-offshore spacing (5–10 km) between CTD stations on each line.

The CODE 1 standard grid consisted of five CTD sections between Elk Creek at 39°07'N and Fort Ross at 38°30'N; the CODE 2 grid differed only in the positions of the most northern section (along 39°03'N) and of the Central line (displaced about 1.6 km (1 mile) south of its CODE 1 position). Each section consisted of 7 or more CTD stations spanning the continental shelf, including at least two stations down to 1000 dbar; on some occasions, the standard sections were extended farther out to sea. A total of five surveys included all five standard sections; these were conducted on April 26–28, 1981; May 20–22, 1981; April 20–22, 1982; May 29–31, 1982; and July 19–22, 1982; a survey conducted on May 2–5, 1981, included only the four standard sections between Point Arena and Fort Ross. Results from these six surveys will be presented below. A seventh survey (including only the four northern sections) was conducted during July 16–19, 1982. All seven surveys included synoptic pairs of Arena and Central line sections, and three additional pairs were occupied on May 23–24, 1981; July 8–9, 1981; and July 13, 1981; the 10 synoptic pairs were used to compare the mean and variability along the Point Arena Line (where the bend in the coastline occurs and the shelf width is about 17 km) to those along the Central line (50 km south of the bend with shelf width of 24 km). Further repeated sections were made along the Central line, and occasional observations were made at many of the other standard stations. All of these observations were used to compute the overall mean fields.

CTD observations were made with a Neil Brown Mark III-B CTD system, using a lowering rate of 45 m min^{-1}. CTD data processing included correcting the conductivity data to agree with in situ calibration samples, filtering to allow for differences in sensor response times, and averaging the calculated salinity and temperature data by 1- or 2-dbar bins. Accuracy of the final processed pressure, temperature, and salinity data is believed to be ± 2 dbar, ± 0.01°C, and ± 0.003 parts per thousand (ppt), respectively. The CTD data have been summarized in reports by *Fleischbein et al.* [1982, 1983*a*, *b*], *Gilbert et al.* [1982], *Huyer et al.* [1984], and *Olivera et al.* [1982].

The current profile data, obtained by means of an Ametek-Straza Doppler acoustic log, typically spanned the 15- to 150-m depth range, with measurements separated vertically by 6.5 m. Estimates of the currents were obtained by filtering the

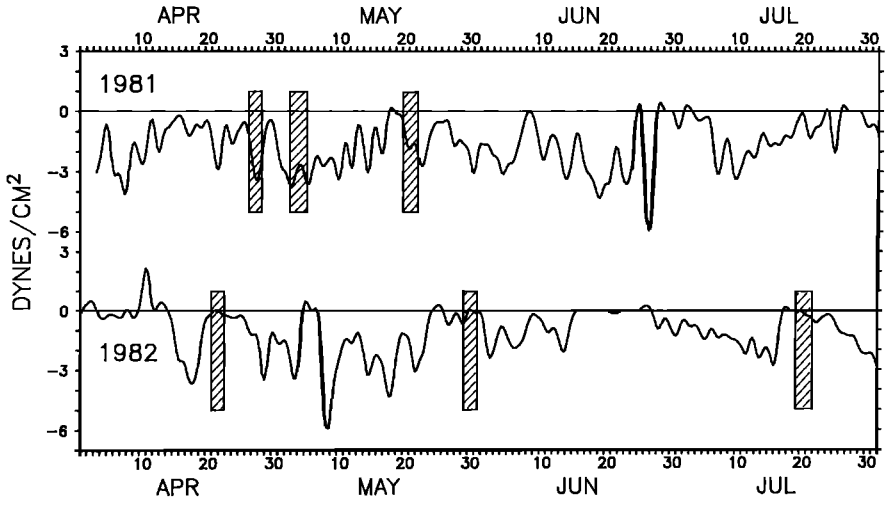

Fig. 2. Time series of the alongshore component of the wind stress at NDBO buoy 46013, moored over the shelf at 38°14'N, 123°18'W, April 1 to July 31, 1981 and 1982. Hatched bars indicate timing and duration of the six synoptic surveys.

combined DAL and navigation (LORAN-C) data over intervals of 30 min. [*Kosro*, 1985].

Shipboard wind speed and direction were recorded at each CTD station, and low-passed ($\omega < 0.6$ cpd) wind stress data computed from hourly wind measurements at NOAA Data Buoy Office buoy 46013 (38°14'N, 123°18'W) were provided by *Halliwell and Allen* [1983, 1985]. Winds were predominantly favorable for upwelling in both years (Figure 2) but periods of very weak winds occurred more frequently in 1982 than in 1981.

3. Synoptic Surveys

The six mesoscale surveys included the four standard sections between Point Arena and Fort Ross: three in 1981, and three in 1982. Although the prevailing winds in spring and summer of both 1981 and 1982 were favorable for upwelling (i.e., southeastward), the surveys in the 2 different years happened to occur during rather different wind conditions (Figure 2). Winds were strong, steady, and favorable for upwelling during each of the three 1981 surveys (Figure 3). In contrast, winds were quite variable during each of the three 1982 surveys, with calms or "light airs" recorded at many CTD stations and moderate or strong winds recorded at others (Figure 3). A previous study of variability along the CODE Central line [*Huyer*, 1984] indicated that surface temperatures across the entire shelf and upper slope, as well as surface salinities over the inner shelf, respond rapidly (within a day) to variations in the alongshore wind stress. Thus we would expect the different winds during the 1981 and the 1982 surveys to be reflected in the observed surface temperature and salinity distributions.

The 1981 surveys all show coldest surface waters adjacent to the coast, and a strong offshore temperature gradient (Figure 4); these are consistent with the strong upwelling-favorable winds. They also show highest salinities occurring inshore (Figure 5). Two of the 1981 surveys showed that inshore waters were colder and more saline in the southern portion of the grid: since the winds were quite steady during both of these surveys, this spatial gradient is probably real.

The three 1982 surveys all show relatively warm surface waters (Figure 4), presumably because of the combination of weak winds and seasonal heating. The climatological monthly mean values of the net downward heat flux for April, May, and July [*Nelson and Husby*, 1983] indicate that seasonal heating would be sufficient to heat a 10-m-deep surface mixed layer by 0.5°C in less than 2 days. The April and July surveys occurred less than 3 days after the cessation of upwelling-favorable winds (Figure 2), and both of these still show surface temperature generally increasing with distance from shore (Figure 4). In contrast, the late May survey occurred after almost a week of unfavorable or very weak winds (Figure 2), and during this survey, warmest waters were observed inshore along the coast.

Like the 1981 surveys, all of the 1982 surveys show relatively fresh water offshore (Figure 5). This low-salinity offshore water mass is generally believed to be advected southward by the California current from a Subarctic origin [*Reid et al.*, 1958]; effluent from the Columbia River (800 km to the north) and discharge from coastal rivers and streams north of Point Arena probably contribute significantly to this water mass [*Huyer*, 1983]. During the July 1982 survey, when local winds were weak and runoff was small, the surface salinity increased nearly monotonically toward the coast just as it did during the three 1981 surveys when upwelling was strong. However, the April and May 1982 surveys show lowest surface salinities in the extreme southeast portion of the grid, adjacent to the coast and near the mouth of the Russian River. These are due in part to the very high local runoff in the spring of 1982: monthly Russian River discharge values for March, April, May, and June 1982 exceed those for 1981 by factors of 2, 13, 4, and 3, respectively [*U.S. Geological Survey*, 1981; *Markham et al.*, 1984]. During both surveys, the low salinities inshore do not penetrate very far below the surface: only during the May survey is there evidence of an inshore salinity minimum and temperature maximum at 20 m (Figures 6 and 7).

During the April 20–22 1982 survey, very low salinity surface water ($S < 32$ ppt) was observed at only one station, but additional observations during the next few days showed salinities as low as 29 ppt just off the Russian River entrance (Figure 8). The low-salinity lens extending 50 km northwest along the coast was extremely thin: at all but one station (just

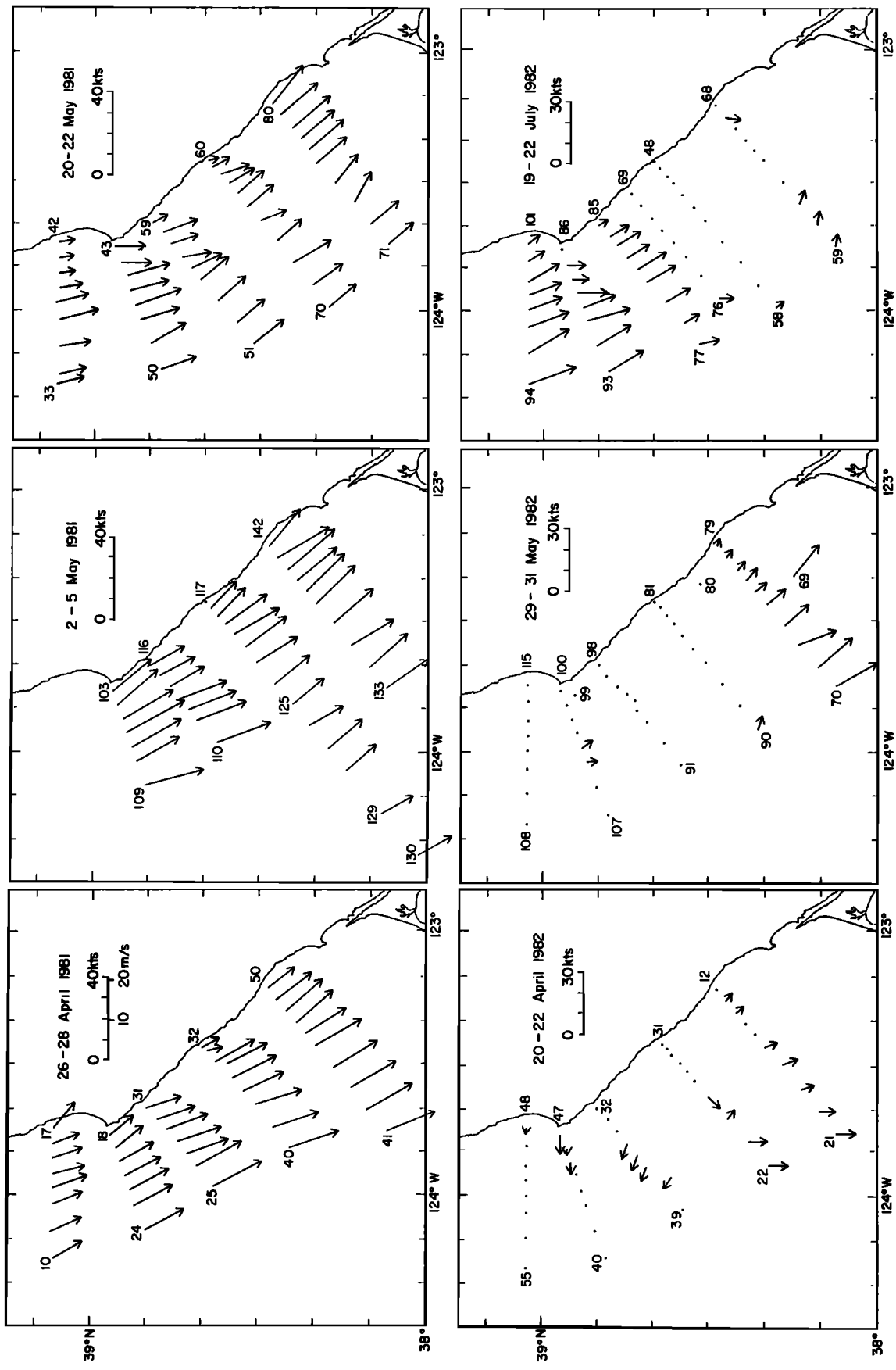

Fig. 3. Shipboard winds at each CTD station during the six synoptic surveys. Dots without vectors indicate light airs or calm conditions. Consecutive CTD station numbers are indicated.

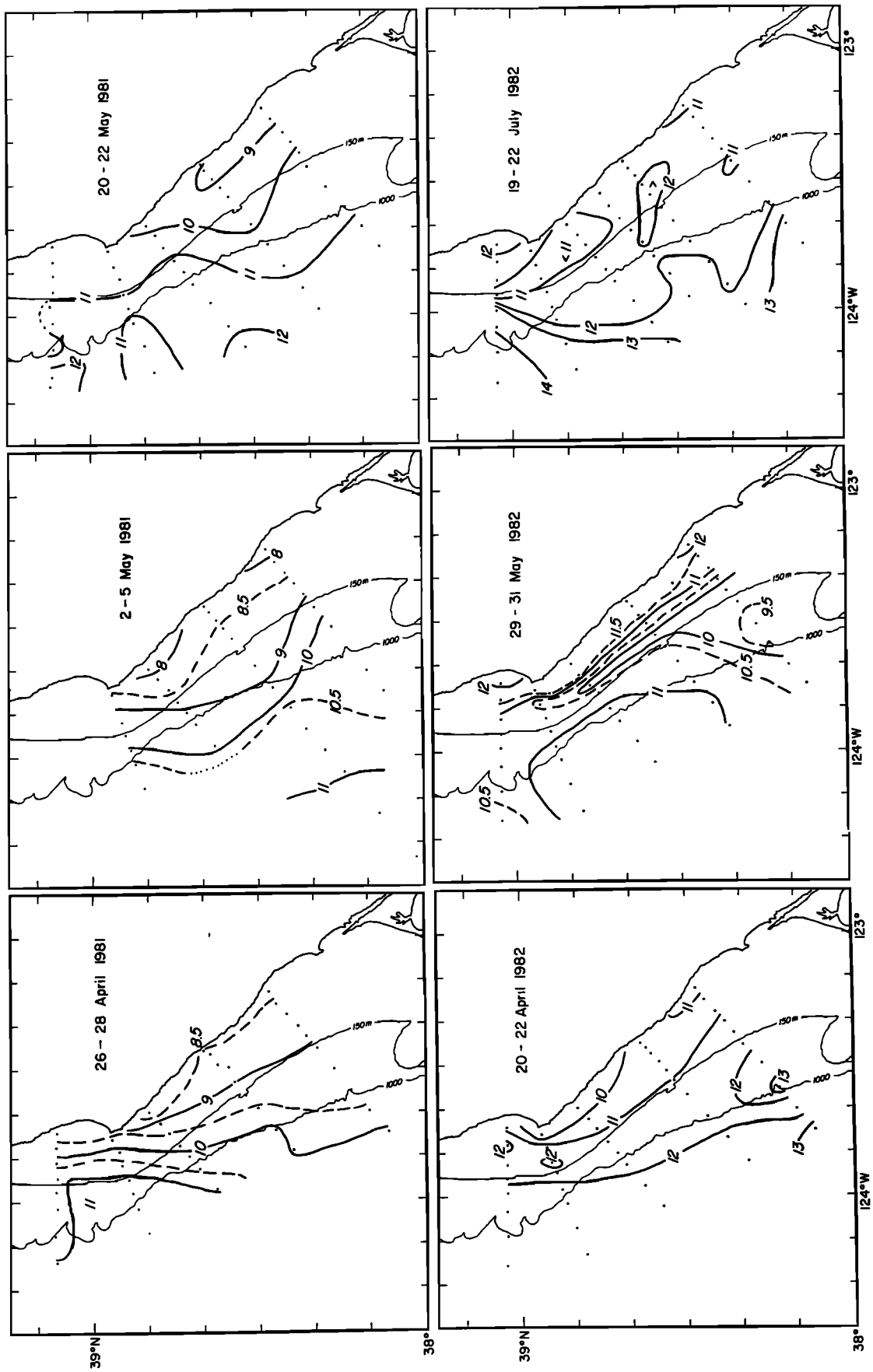

Fig. 4. Maps of sea surface temperature (in degrees Celsius) during the six mesoscale surveys.

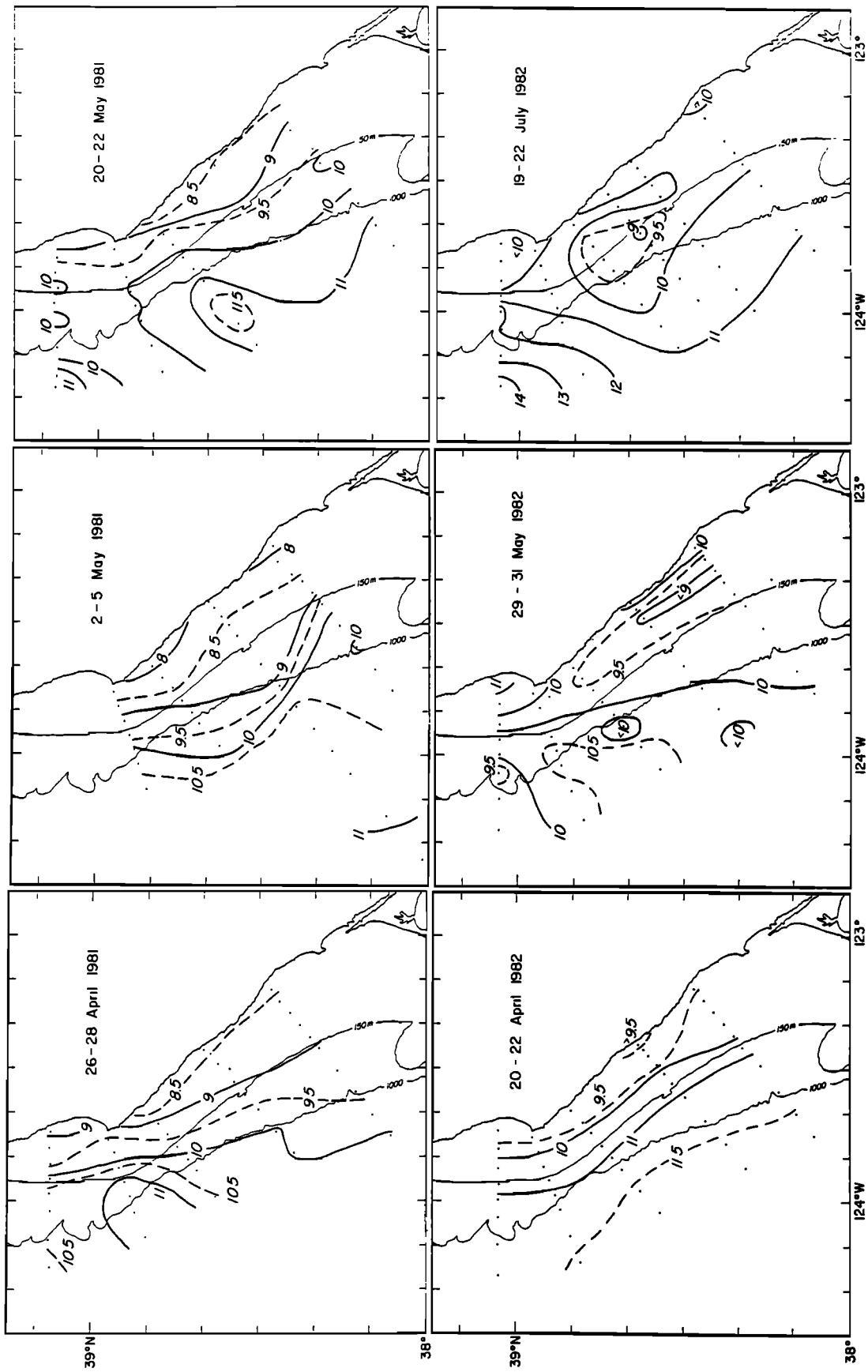

Fig. 5. Maps of surface salinity (in parts per thousand) during the six mesoscale surveys.

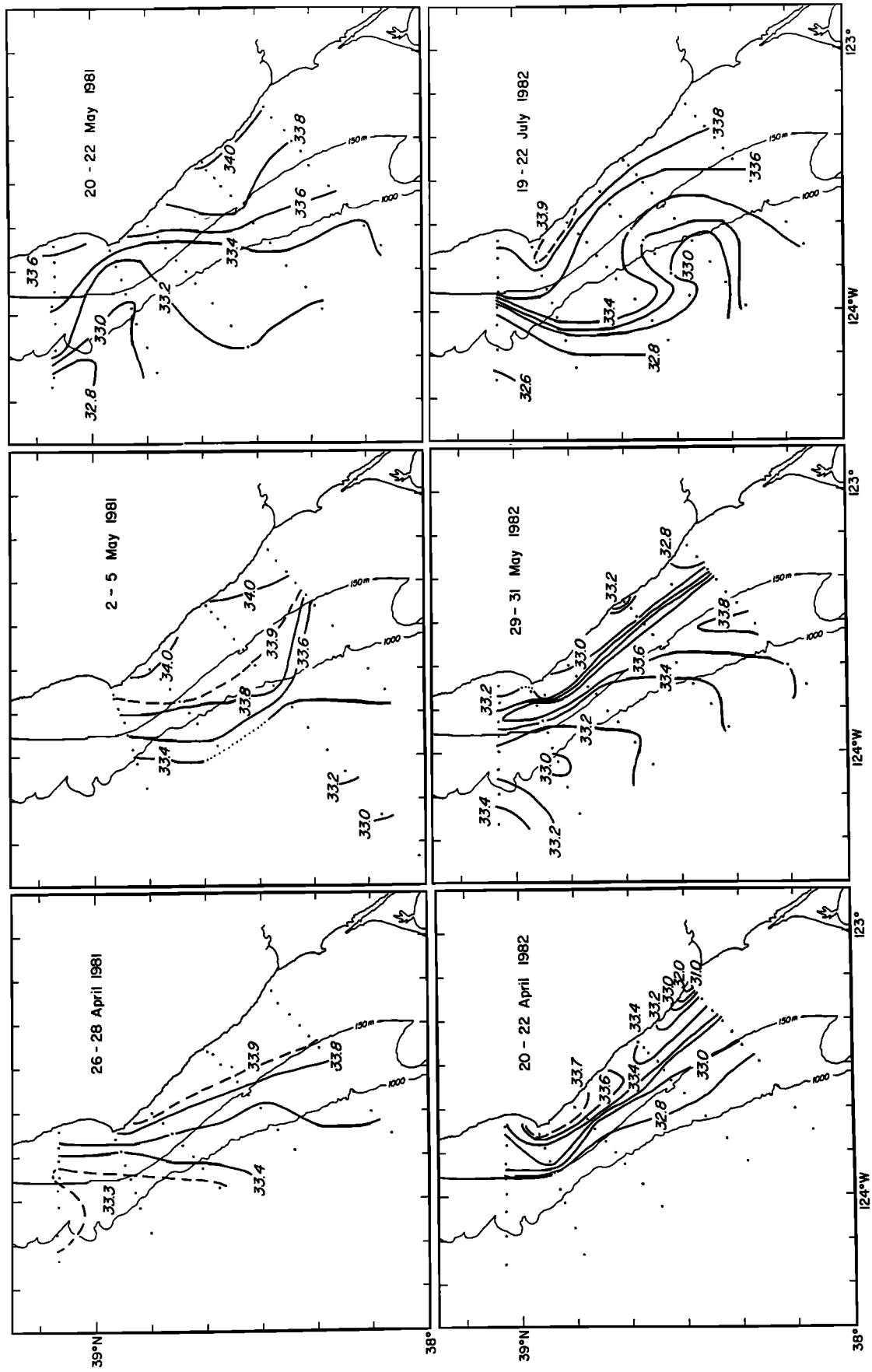

Fig. 6. The temperature distribution (in degrees Celsius) at 20 m during each of the six mesoscale surveys.

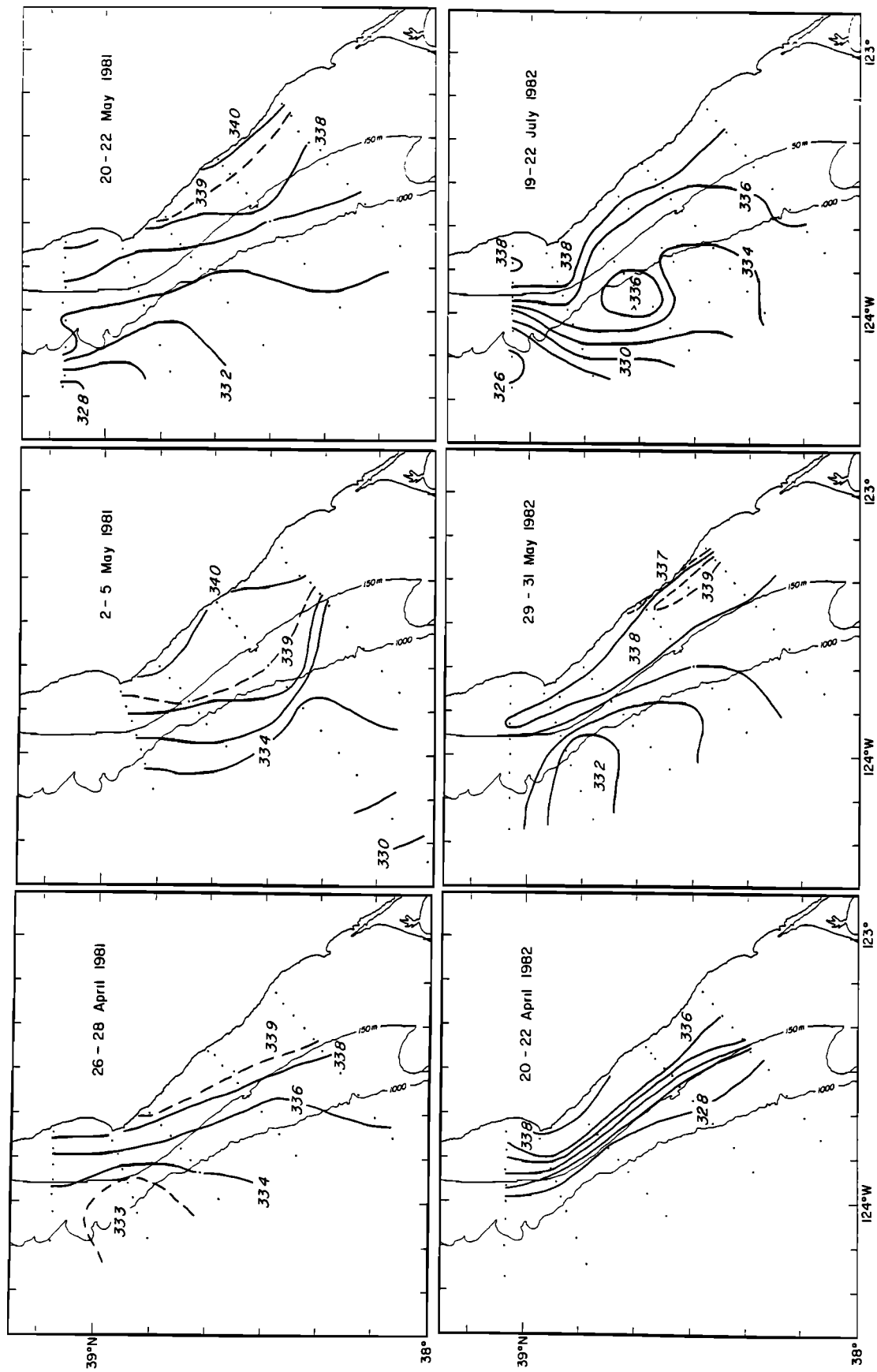

Fig. 7. The salinity distribution (in parts per thousand) at 20 m during each of the six mesoscale surveys.

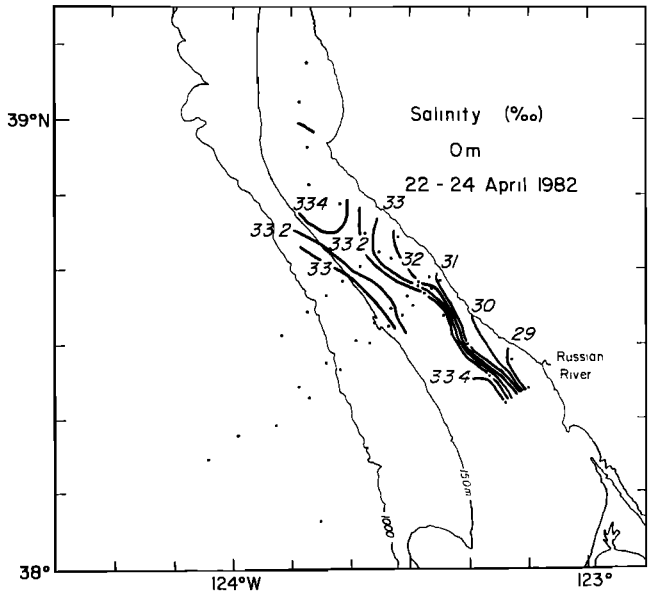

Fig. 8. Surface salinity distribution during April 22–24, 1982.

off the Russian River entrance) the salinity at 10 m exceeded 33 ppt. The Russian River discharge between April 17 and 24 was 9.45×10^7 m^3. If the anomalous portion of the salinity profile is modeled as varying linearly from an average surface value of 31.5 ppt to an undisturbed "deep" value of 33.5 ppt, the Russian River discharge can explain a lens 8 km wide, 50 km long, and 8 m thick. These dimensions are close to the observed values. The apparent poleward displacement of the 33-ppt isohaline at the surface by about 40 km between April 21 and 23 agrees well with the 2-day average alongshore current measured at moorings over the inner shelf (e.g., 24 cm s^{-1} at a depth of 20 m at R2 (38°27'N, 123°14'W) [*Beardsley and Alessi*, 1985].

The May 29–31, 1982, survey showed a much longer lens of low-salinity water extending along the coast past Point Arena. Again, the probable origin of much of this inshore fresh water is the Russian River. Between April 28 and May 22 the average surface current at station R2 (at 38°27'N, 123°14'W) was near zero [*Winant et al.*, 1985]; meanwhile, the Russian River discharged 80×10^6 m^3 [*Markham et al.*, 1984]. Between May 23 and 30 the average near-surface currents over the inner shelf were about 20 cm s^{-1} poleward (Figure 9), sufficient to advect some of the low-salinity surface water well past Point Arena by May 31. The width of the coastal strip of low-salinity water is about the same as the width of the poleward flow (Figure 9). The equivalent amount of fresh water in this narrow coastal strip (assuming a well-mixed lens with $S = 32.9$ ppt 8 km wide, 80 km long, and 5 m deep and a "deep" salinity of 33.9 ppt) is similar to the total Russian River discharge between April 28 and May 30; the average depth of the lens may have exceeded 5 m, and some of the fresh water was probably supplied through San Francisco Bay. The inshore low-salinity lens disappeared very quickly after strong upwelling-favorable winds resumed on June 1: there was no evidence of it during a June 2–3 shelf survey; instead, surface salinities adjacent to the coast exceeded 33.8 ppt [*Fleischbein et al.*, 1983*b*], as is usual during strong upwelling (e.g., during the 1981 surveys in Figure 5). Thus it appears that the inshore low-salinity lens is a transient feature, observed only when local runoff is substantial and local winds are not favorable for upwelling.

For each of the mesoscale surveys, we computed the geopotential anomaly (ΔD) of the sea surface relative to 100 dbar (Figure 10). In each survey, most of the CTD stations were beyond the 100-m isobath; for the few shallower stations, we calculated $\Delta D_{0/p_{max}}$ directly and $\Delta D_{p_{max}/100}$ by linear extrapolation from the next offshore pair of stations to obtain $\Delta D_{0/100}$ (following *Reid and Mantyla* [1976]). The resulting distributions of geopotential anomaly (Figure 10) are very similar to the near-surface salinity maps (Figures 5 and 7). Highest values coincide with the low-salinity waters offshore, and lowest values are associated with the high-salinity freshly upwelled waters near shore; inshore values were relatively high during the May 1982 survey when the freshwater lens lay over the inner shelf. Thus the geostrophic flow is generally along isohalines, with the low-salinity waters to the right; a similar correspondence between the geostrophic shear and surface salinity gradients has also been observed farther from shore [*Kosro and Huyer*, 1986].

The surface geostrophic flow relative to 100 dbar was generally equatorward over the outer shelf and upper slope (Figure 10). Simple models of coastal upwelling in a stratified ocean [e.g., *Allen*, 1973] usually produce a baroclinic, equatorward coastal jet between the dense, freshly upwelled water inshore and the lighter water offshore. This baroclinic jet was manifested in classical form during the April 20–22, 1982, survey: both its strength and the position of its core (over the shelf break) were nearly uniform over the 100-km alongshore extent of the survey region (Figure 10). This classical two-dimensional form of the jet, with a clearly defined core and negligible alongshore gradients, was not observed during any of the three 1981 surveys made during strong upwelling-favorable winds nor during the subsequent 1982 surveys.

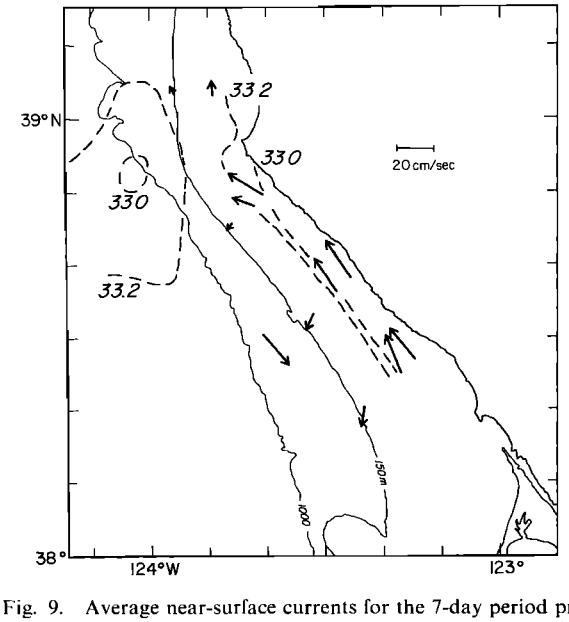

Fig. 9. Average near-surface currents for the 7-day period preceding the May 29–31 survey calculated from data obtained by the CODE 2 moored array [*Beardsley et al.*, 1985, *Winant et al.*, 1985]. The dashed and dashed-dotted lines indicate the surface position of the 33.0-ppt and 33.2-ppt isohalines, respectively.

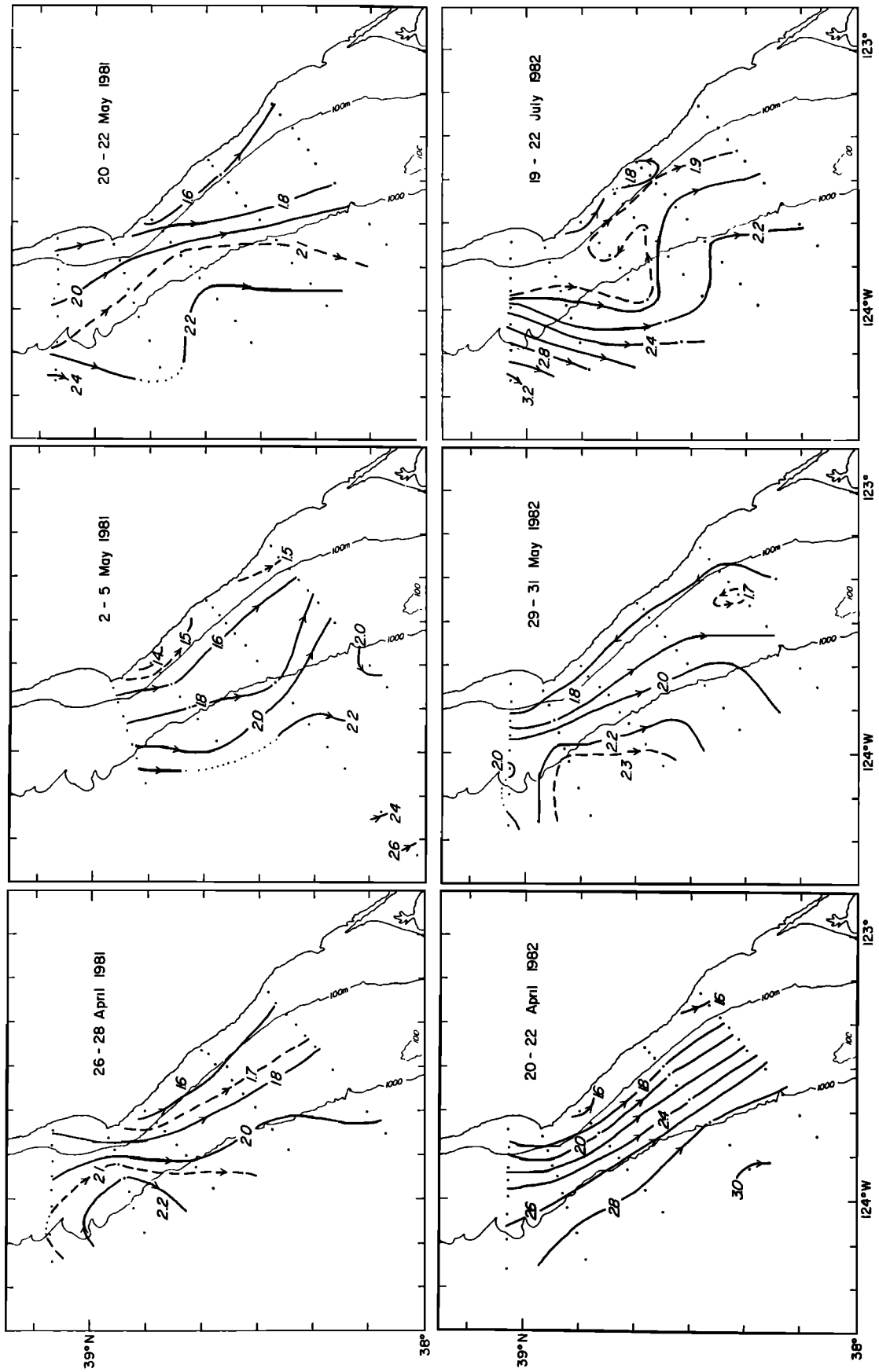

Fig. 10. Maps of the geopotential anomaly ($m^2 s^{-2}$) of the sea surface relative to 100 dbar each of the six mesoscale surveys.

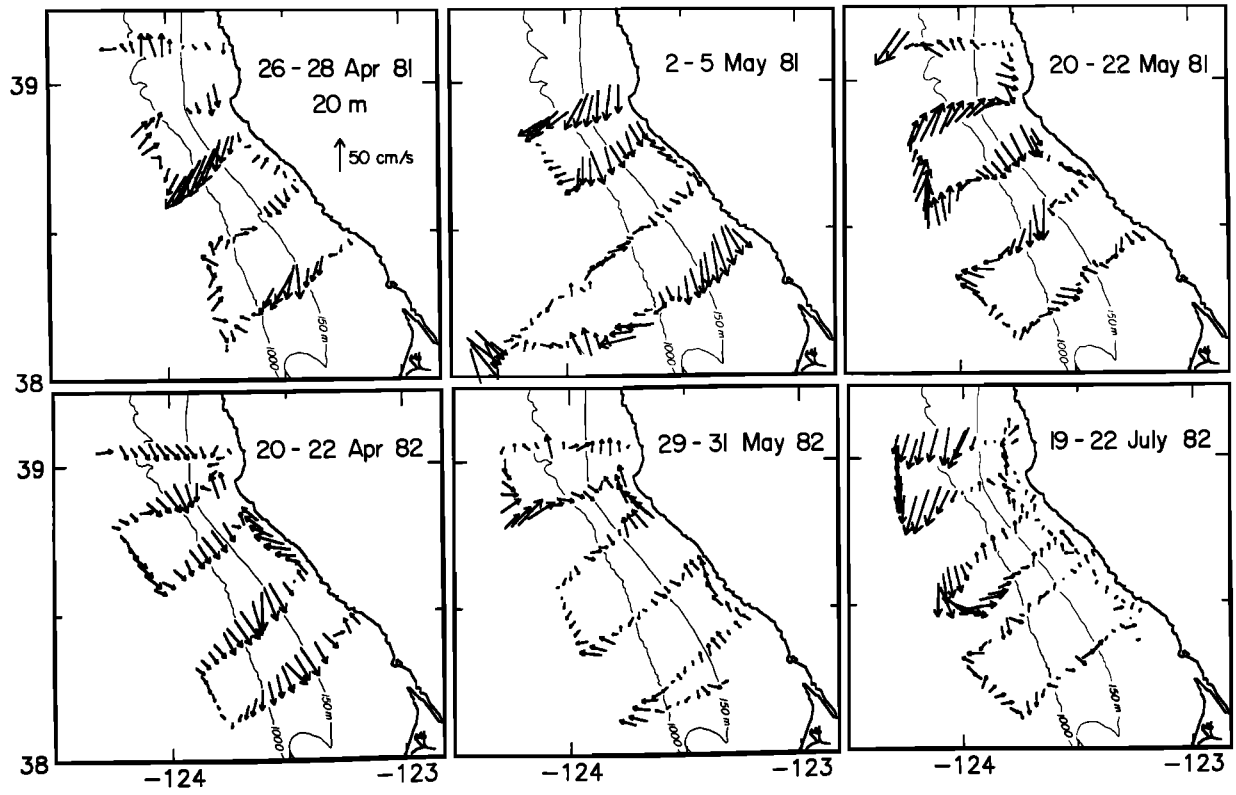

Fig. 11. Maps of DAL current vectors at a depth of 20 m for each of the six mesoscale surveys.

There is some indication of an equatorward jet in the geostrophic current field during all of the surveys, but its strength and offshore position vary considerably within the survey region and from one survey to another. During the April 1981 and May 1982 surveys, the geostrophic jet is strongest and nearest shore off Point Arena; in late May 1981, strongest geostrophic currents are observed south of Point Arena. During the July 19–22, 1982, survey, a geostrophic jet is present only in the extreme northwest corner of our survey region. Maps of current vectors from the moored array [*Beardsley and Alessi*, 1985] suggest continuity between this southwestward jet and very strong (>50 cm s^{-1}) southward surface currents observed over the shelf north of Point Arena during July 12–17; satellite images and an offshore survey indicate that the jet turns westward and continues out to sea for at least 200 km [*Kosro and Huyer*, 1986].

Most of the geopotential anomaly maps (Figure 10) suggest that gradients in the alongshore direction are much weaker than those in the onshore-offshore direction. This may be due, at least in part, to our biased sampling plan: since the spacing between adjacent sections was 20–30 km, the dynamic topography cannot resolve eddies or meanders with alongshore scales of less than 40–60 km. Except for April 1982, all of the surveys show evidence for meanders or eddies of this dimension; their presence or absence does not seem to be related to the strength of the upwelling-favorable winds (compare Figures 3 and 10).

The current vectors measured by the Doppler acoustic log also show substantial variations in the flow pattern. Maps are shown for three different levels: at a depth of 20 m, our shallowest common level (Figure 11); at 80 m, about the middle of our depth range (Figure 12); and at 150 m, our deepest common level (Figure 13). These maps can resolve eddies or meanders with alongshore scales as small as the separation between adjacent sections, i.e., 20–30 km. Three different phenomena seem to dominate at one time or another: a baroclinic equatorward jet, an inshore poleward countercurrent, and eddies or meanders of various scales. Several surveys show some combination of these three phenomena.

Maps of the DAL current vectors (Figures 11–13) clearly show the classical two-dimensional structure of the equatorward baroclinic jet during the April 1982 survey: at 20 m (Figure 11), maximum velocities (>50 cm s^{-1}) were observed along the upper continental slope, about 25 km from the coast. At 80 m (Figure 12), the core of the jet lay farther from shore (at about 40 km) and maximum velocities were considerably weaker (<30 cm s^{-1}); *Kosro*'s [this issue] vertical sections show that the jet did not penetrate below about 100 m, and a coherent equatorward current is not present at 150 m (Figure 13). Relative geostrophic velocities were calculated by objective mapping [*Bretherton et al.*, 1976] of the $\Delta D_{20/80}$ field using an exponentially damped cosine covariance function with a wavelength of 95 km and a decay scale of 30 km; these parameters were determined by fitting a damped cosine function to the average of the covariance functions computed from all 13 (partial and complete) mesoscale surveys. These objectively mapped geostrophic velocities are in excellent agreement with the observed DAL velocity difference vectors (Figure 14); the magnitude of the complex correlation between these vector fields is 0.81. During the May 2–5, 1981, survey the coastal jet was manifested as a broad equatorward current over the continental shelf and upper slope (Figure 11). This

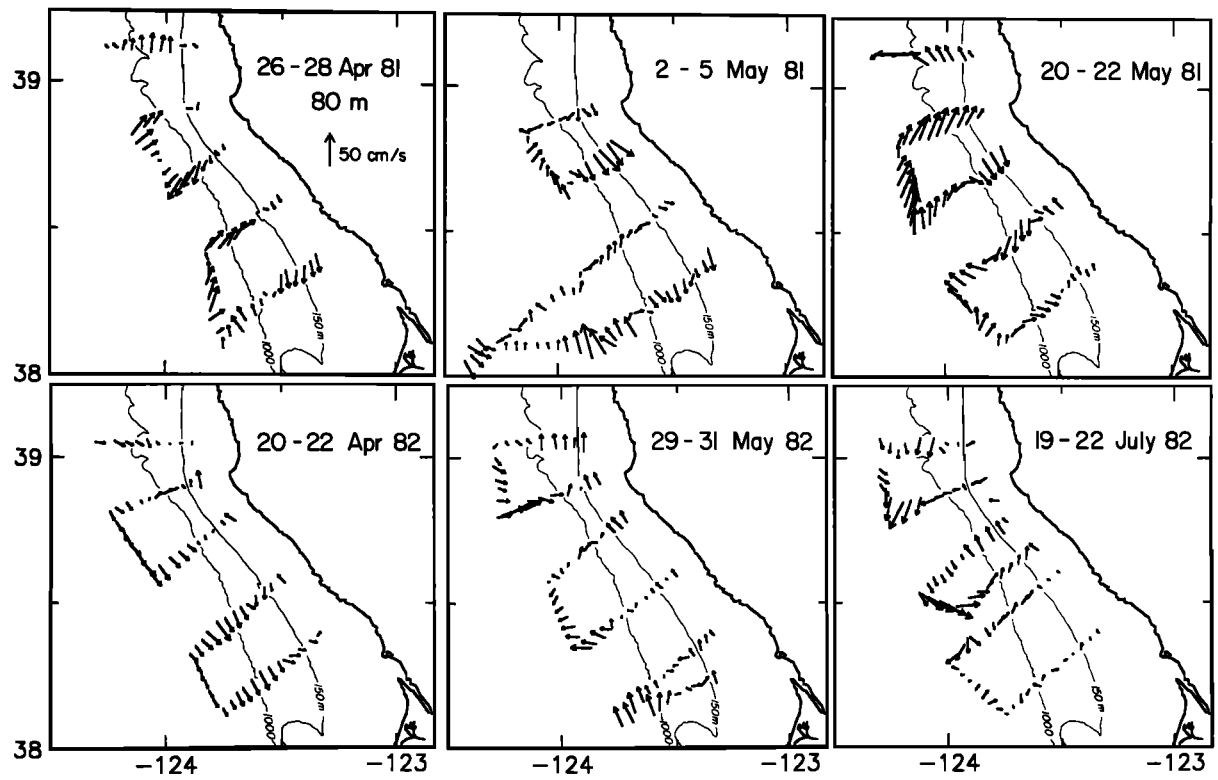

Fig. 12. Maps of DAL current vectors at a depth of 80 m.

current did not have a well-defined core, and maximum velocities varied considerably along the coast, from less than 30 cm s^{-1} on the Central line to more than 60 cm s^{-1} on the Ross line; it is weakest on the Central line where the geostrophic streamlines (Figure 10) are farthest apart. During this same survey, the current seems to divide off Point Arena: one branch continues southeastward along the coast and the other turns directly offshore; this split is seen very clearly in the tracks of surface drifters deployed on May 2, 1981 (Figure 15; see also *Davis* [1983]). During the July 1982 survey (Figures

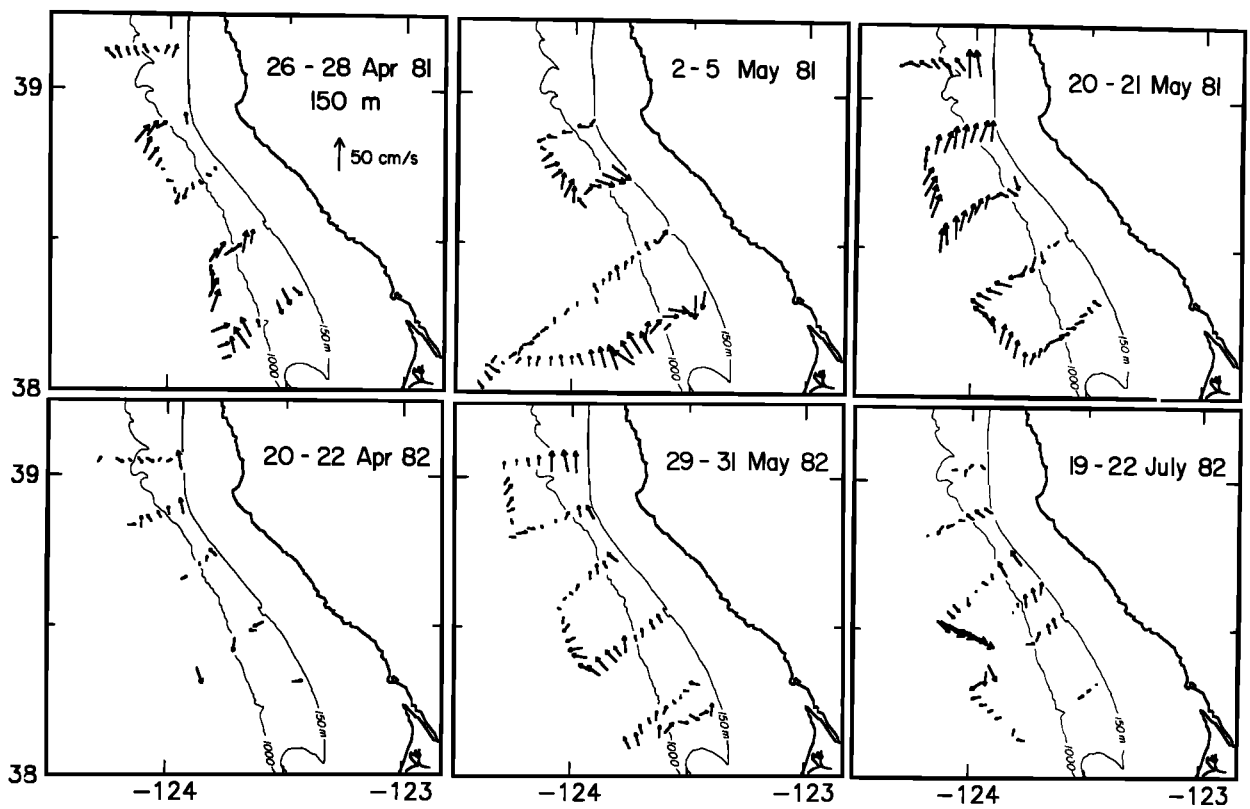

Fig. 13. Maps of DAL current vectors at a depth of 150 m. Note that not all DAL profiles penetrated to this depth.

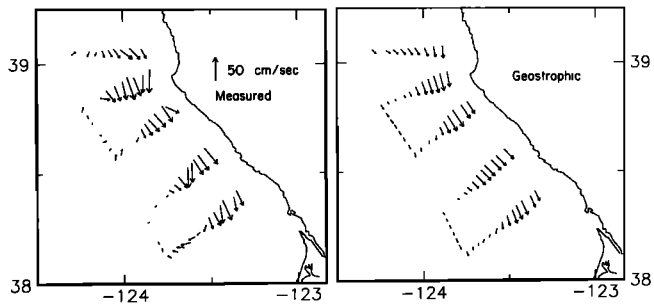

Fig. 14. Maps of the (left) measured and (right) geostrophic velocity differences between 20 and 80 m during April 20–22, 1982. Measured differences were calculated directly from DAL data. Geostrophic velocity differences were obtained from objective mapping of the geopotential anomalies between 20 and 80 dbar.

12 and 13), the coastal jet was farther from the coast; very strong southwestward currents (>70 cm s^{-1} at 20 m and >30 cm s^{-1} at 80 m) were measured in the northwestern portion of the grid, in good agreement with the dynamic topography there (Figure 10).

The DAL maps for the April 26–28, 1981, May 20–22, 1981, and May 29–31, 1982, surveys (Figure 11) do not show clear evidence of a continuous equatorward current although the dynamic topography during each of these surveys (Figure 10) indicated a meandering but rather weak (<20 cm s^{-1}) baroclinic jet. Instead, each of these surveys shows the presence of one or more circular or elongated eddies. A particularly obvious example with tangential velocities in excess of 50 cm s^{-1} was observed on May 20–22, 1981: an anticyclonic circular eddy with its northeastern limb flowing onto and over the shelf was centered over the continental slope at 38.6°N, 123.8°W. Neither its apparent radius (≈ 30 km) nor its position seemed to vary with depth between 20 and 150 m (Figures 11–13). Tangential velocities decreased by only a factor of about 2 in the upper 150 m; both geostrophic and measured shears were much smaller than those observed in the coastal jet during the April 1982 survey. The July 19–22, 1982, survey (Figure 11) also showed an eddy centered over the continental slope (at 38.7°N, 124.0°W); this eddy was asymmetrical (its offshore, southward limb had much stonger velocities than its inshore, northward limb) and elongated (at 20 m its alongshore axis was about twice as long as its onshore-offshore axis). At 80 m and 150 m it seems more nearly circular (Figures 11 and 12). Surface drifters and 30-m drogues deployed on July 15 and 18, 1982 [*Davis*, 1983], confirm the presence of an elongated, asymmetrical eddy centered over the continental slope; there is reasonably good agreement between drogue velocities and DAL measurements (Figure 16). Small-scale, more confused eddylike features were observed over the slope and the entire shelf during April 26–28, 1981; over the slope and outer shelf during May 29–31, 1982; and in the southern portion of the July 1982 survey (Figure 12). All of these eddies seem to penetrate down to at least the 150-m level (Figure 13), considerably deeper than the baroclinic coastal jet.

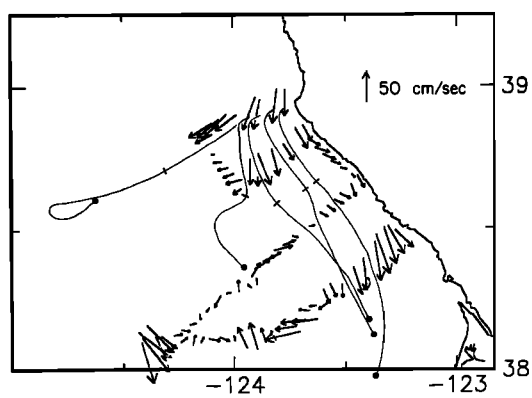

Fig. 15. Surface drifter tracks superimposed on the DAL 20-m velocity field for the May 2–5, 1981, survey. Drifters were deployed off Point Arena on May 2, 1981, and positions were determined about once a day [*Davis*, 1983]. Drifter positions 1 day and 3 days after deployment are indicated by ticks and dots, respectively.

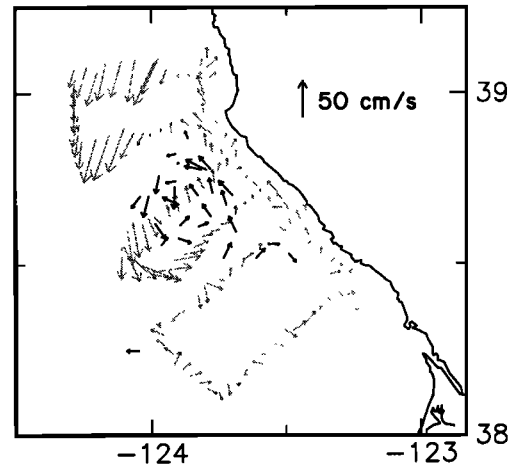

Fig. 16. Velocities of 30-m drogues (solid arrows) superimposed on the DAL 20-m velocity field (stippled arrows) for the July 19–22, 1982, survey. Drogues were deployed on July 15 and 18, and positions were determined once or twice per day [*Davis*, 1983]. Drogue velocity vectors were calculated from successive drogue positions within the July 19–22, 1982, period.

A narrow (<15 km wide) poleward countercurrent was observed along the coast during each of the three 1982 surveys when winds were weak (Figure 11). In each case, strongest poleward currents were observed at locations nearest the coast, within 5 km from shore. *Kosro* [1986] shows that this inshore countercurrent is very nearly barotropic. No continuous inshore countercurrent was observed during the three 1981 surveys with strong upwelling-favorable winds, but poleward flow was observed at the inshore end of the Central line at the beginning of the May 20–22, 1981, survey which was preceded by several days of very weak winds (Figure 2). The countercurrent observed on May 29–31, 1982, disappeared rapidly after upwelling-favorable winds resumed on June 1: it was not observed during a survey of the shelf on June 2–3. The apparent relation between the nearshore currents and the wind is confirmed by data from the CODE 2 moored array: linear regression analysis between the alongshelf component of the vertically averaged current at each mooring and the alongshore wind stress over the midshelf shows that currents over the inner shelf are poleward in the absence of wind stress and equatorward when the wind stress is favorable for upwelling [*Winant et al.*, this issue]. Similar analysis using the wind stress at NDBO buoy 46013 and the principal axis component of the near-surface currents (depths of 10 or 20 m) from both the CODE 1 and CODE 2 moored arrays shows that in the absence of local winds the poleward countercurrent is about 15 km wide (Figure 17); its strength was about the same in both years. With stronger local winds, the countercurrent is both narrower and weaker; with an equatorward wind stress of 1.5 dyn cm^{-2} it is barely discernible (Figure 17). The

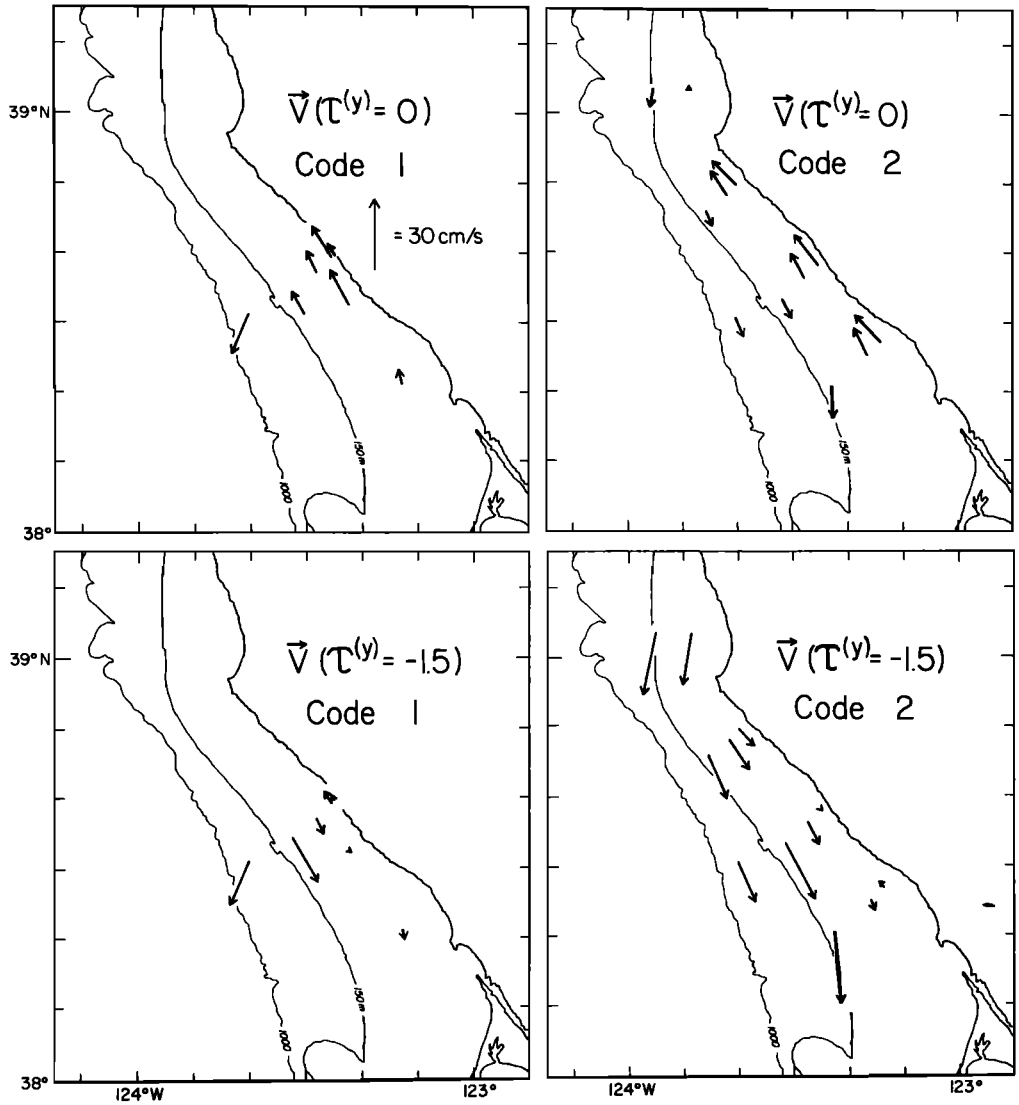

Fig. 17. Near-surface current vectors expected at (left) the CODE 1 and (right) the CODE 2 current meter moorings, (top) in the absence of local wind-driven upwelling and (bottom) when the local alongshore wind stress is -1.5 dyn cm^{-2}. These expected currents were calculated from simple linear regression of the principal axis component of the current on the wind stress, with the current data lagging by 12 hours.

countercurrent is clearly important for the northward advection of local runoff and Russian River discharge along the coast. Whether it is continuous along the coast past Point Arena and Point Reyes is not known at this time.

4. Structure of the Average Fields

Average temperature, salinity and density fields were calculated in two different ways, yielding "synoptic average" and "overall average" fields. Synoptic averages were computed from the six synoptic surveys described above (Figures 3–7), using only stations which were occupied during all six surveys. These average fields do not extend north of Point Arena and consist of only 33 standard stations (7, 7, 9, and 10 stations on the Arena, North, Central, and Ross lines, respectively). Overall averages were computed from all CTD data obtained at any of the standard station positions during the six hydrographic cruises (CODE 1 legs 4, 5, 7 and 7 and CODE 2 legs 6, 8, and 9, see section 2 for dates); these include the six synoptic surveys and also additional partial surveys, repeated sections, and occasional observations. Pairs of stations over similar isobaths on the Elk line at 39°07'N and Irish Gulch line at 39°03'N were combined to yield overall average stations along 39°05'N. Similarly, data from the slightly different CODE 1 and CODE 2 Central lines were combined. The

TABLE 1. Correlation (r) and Regression (b) Coefficients Calculated From a Simple Linear Regression, $y = a + bx$, of the Overall Average y on the Synoptic Average x, for Temperature, Salinity, Density, and Geopotential Anomaly at Selected Depths

Depth, m		Temperature		Salinity		σ_θ		$\Delta Dz/100$		
	N	r	b	r	b	r	b	N	r	b
5	33	0.96	1.04	0.95	0.97	0.96	1.01	23	0.99	0.96
30	32	0.99	1.02	0.99	0.98	0.99	1.00	23	0.99	0.93
50	29	0.99	0.98	0.99	0.96	0.99	0.97	23	0.99	0.90
100	23	0.97	0.85	0.99	0.86	0.99	0.86			
150	16	0.97	0.97	0.98	0.83	0.97	0.87			
200	13	0.99	0.99	0.94	0.74	0.96	0.87			

Since many grid points are in shallow water, the number of pairs (N) decreases with increasing depth.

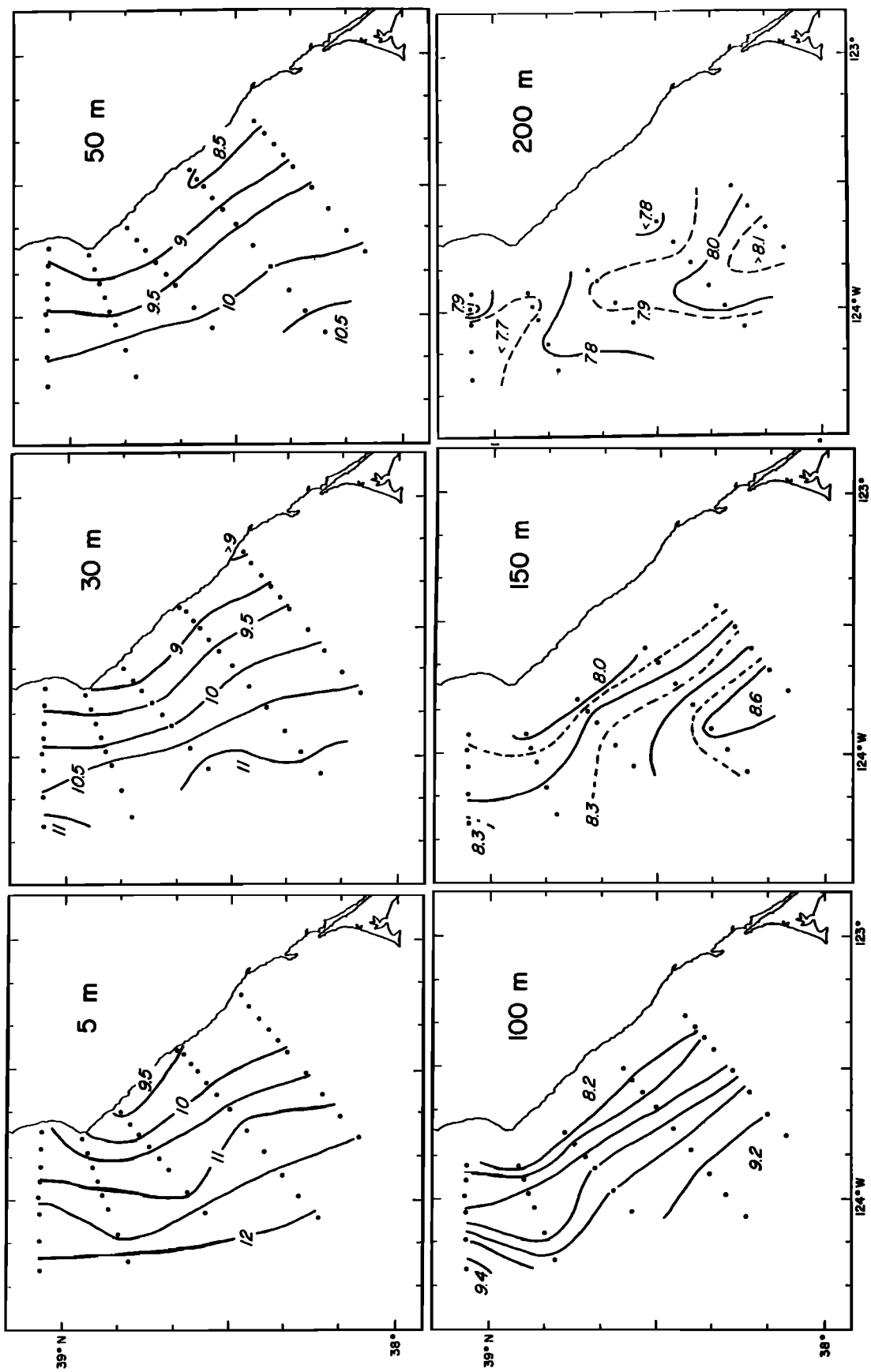

Fig. 18. The overall average temperature distributions (in degrees Celsius) at selected depths: 5, 30, 50, 100, 150, and 200 m.

resulting fields have 46 grid points with six or more occupations each. The overall average fields have the advantage of greater spatial coverage: they extend both farther north and farther offshore than the synoptic average fields. They have the disadvantage that their apparent spatial structure may be aliased by temporal sampling differences. However, comparison of the synoptic and overall fields in the region where they overlap showed them to be very similar: correlation and regression coefficients between them are very close to 1 (Table 1). This similarity implies that the possible aliasing is not important, and thus we use the overall fields to describe the average spatial structure of the upwelling regime near Point Arena.

Maps of the average temperature field at selected depths (Figure 18) show that the near-surface temperature increases monotonically with distance from shore. This suggests that the upwelling induced by the mean equatorward wind stress is strongest in a narrow band adjacent to the coast, which is consistent with the analysis of repeated Central line sections [*Huyer*, 1984]. The offshore temperature gradient decreases with depth from about 0.05°C km^{-1} at a depth of 5 m to about 0.03°C km^{-1} at 100 m. Near the surface (at both 5 and 30 m), there is tendency for isotherms to diverge from the coast: warmer waters lie nearer shore in the north. Isotherms at 50 and 100 m generally parallel the coastline. At 150 m, inshore temperatures are still uniformly cold, but offshore waters are considerably warmer in the south. Average temperatures at 200 m do not show a consistent offshore gradient; instead, the field is dominated by a weak alongshore gradient, with warmest waters occurring in the south. The tonguelike structure in the southern portion of the grid at both 150 m and 200 m is suggestive of northward advection.

Maps of the average salinity field at the same depths (Figure 19) all show a virtually monotonic onshore gradient, with highest salinities occurring inshore. There are three exceptions: (1) some very low salinity surface water occurs at the inshore end of the Ross line, presumably a signature left by the time-varying Russian River plume; (2) a meander in one of the isohalines near the end of the Central line is observed at all depths between 5 and 100 m; and (3) at 200 m a small local salinity maximum on the Ross Line coincides with the local temperature maximum there. The magnitude of the onshore salinity gradient does not change much between 5 and 50 m, but below 50 m it decreases substantially with increasing depth; the gradient is still present though barely discernible at 200 m. In the upper layers, the isohalines diverge from the coast even more clearly than the isotherms, with relatively fresh water observed in the northwest portion of the grid. The low-salinity pool just off Point Arena seems to be a persistent feature (Figure 7); the available data indicate that the associated north-south surface salinity gradient can extend more than 250 km out to sea [*Kosro and Huyer*, 1986]. There is a weak north-south gradation of mean T-S characteristics in the region: along the offshore boundary of the grid, waters of a given salinity are warmer in the south than in the north. There is also an onshore-offshore gradient in T-S characteristics, particularly in the northern portion of the grid.

The structure of the average density field (Figure 20) is very similar to the salinity structure: density increases nearly monotonically toward shore at all levels above 200 m. As in the salinity field, there are exceptions to this monotonic increase: there is low-density surface water in the southeastern corner, presumably associated with the Russian River plume, and there is a meander in the near-surface isopycnals near the offshore end of the Central line. Note that the map of density at 200 m, unlike the corresponding salinity map, does not show any local extrema: even at this depth the density increases monotonically toward shore. This positive horizontal density gradient implies a negative vertical shear. If the warm tongue in the 150- and 200-m temperature distributions (Figure 18) is due to advection by a geostrophic undercurrent, its core must lie below 200 m.

Maps of the average geopotential anomaly referenced to 100 and 500 dbar (Figure 21) were prepared using only data from CTD casts to at least the reference depth. These maps show a weakly meandering equatorward current over the upper continental slope. Its core velocity decays rapidly with depth, from about 25 cm s^{-1} at 5 m to 15 cm s^{-1} at 50 m and about 5 cm s^{-1} at 100 m. Note that the average core velocities at the surface are considerably smaller than those observed during a particular survey (compare Figure 10). Both the 150-m and the 200-m maps show a generally noisy field, with several local extrema; they show neither a well-defined southward flow nor a continuous poleward undercurrent. The geostrophic streamlines near the surface diverge gradually from the coast; this divergence inplies an average alongshore pressure gradient and associated weak (< 2 cm s^{-1}) offshore flow.

Elsewhere in this volume, *Kosro* [this issue] gives a full discussion of the structure of the average velocity field as measured by the Doppler acoustic log. Here we show maps of average velocity vectors at selected depths (Figure 22) for comparison with the individual synoptic surveys (Figures 11–13) and with the average hydrographic fields (Figures 18–21). These maps were obtained by averaging all DAL velocity observations at each standard station position shown in Figure 1 and at additional station positions over the 50-fm (90 m) and 100-fm (180 m) isobaths [*Kosro*, 1985]; each average velocity vector represents at least eight observations. The average DAL velocity field (Figure 22) shows most of the main features seen in the individual synoptic surveys (Figures 11–13): baroclinic equatorward flow in the upper layers, weak poleward flow near the surface at the inshore end of the Central line, and weak poleward flow shelf break at a depth of 150 m. The latter is more obvious in the average field than in the individual surveys. The eddies and meanders that dominated the velocity field during most of the synoptic surveys are generally absent from the average field. Only in the southwestern portion of the grid is there any evidence of a weak meander or eddy in the mean field.

The average DAL velocities at a depth of 20 m (Figure 22) show a broad equatorward flow with a weak maximum over the upper continental slope. Core velocities of about 20 cm s^{-1} are in reasonable agreement with the average dynamic topography at 5 and 30 m (Figure 21). These average core velocities are considerably smaller than those of the classical coastal jet observed during the April 1982 survey (Figure 11). Nevertheless, the equatorward surface flow in the average DAL current field is a good approximation to a two-dimensional, baroclinic coastal jet in geostrophic balance: Figure 23 shows good agreement between the 20-m minus 80-m difference vectors calculated directly from the DAL averages and the corresponding geostrophic velocity vectors obtained from the average geopotential anomaly field using the same objective mapping technique as was used for Figure 14; the complex correlation coefficient between these fields is 0.63. Over the shelf, the strength of the average southward

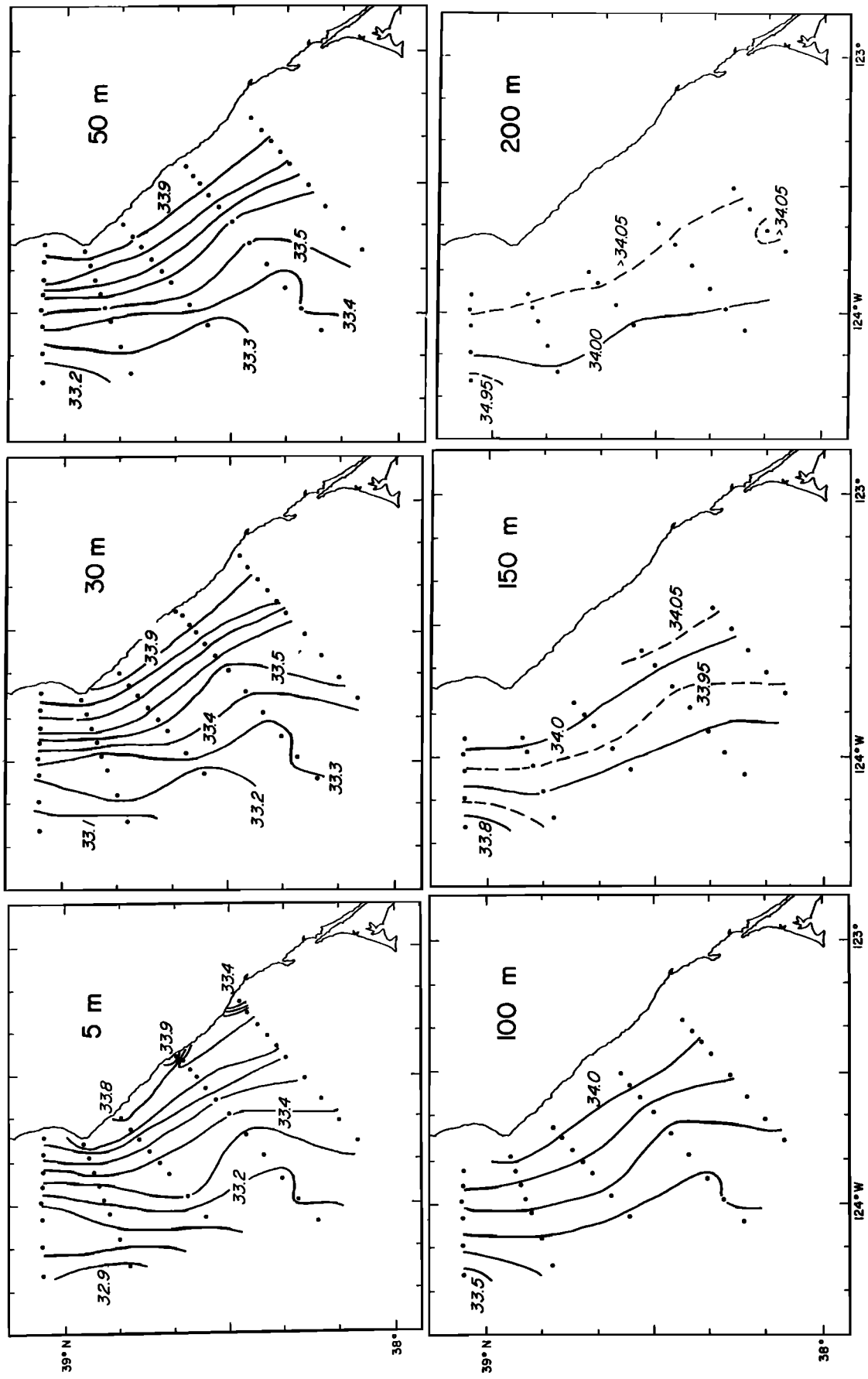

Fig. 19. The overall average salinity distributions (in parts per thousand) at selected depths: 5, 30, 50, 100, 150, and 200 m.

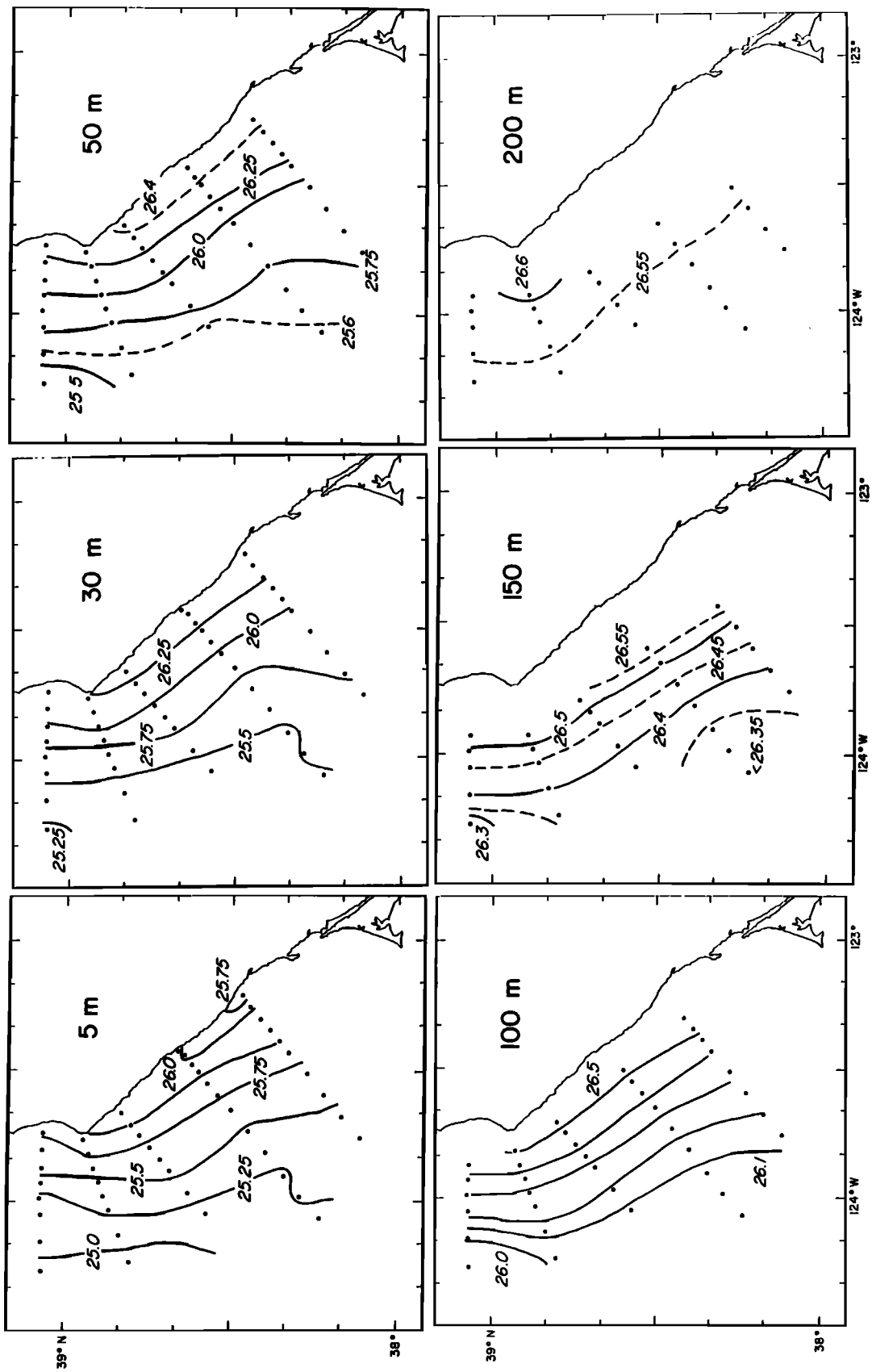

Fig. 20. The overall average of the density anomaly σ_θ at selected depths: 5, 30, 50, 100, 150, and 200 m.

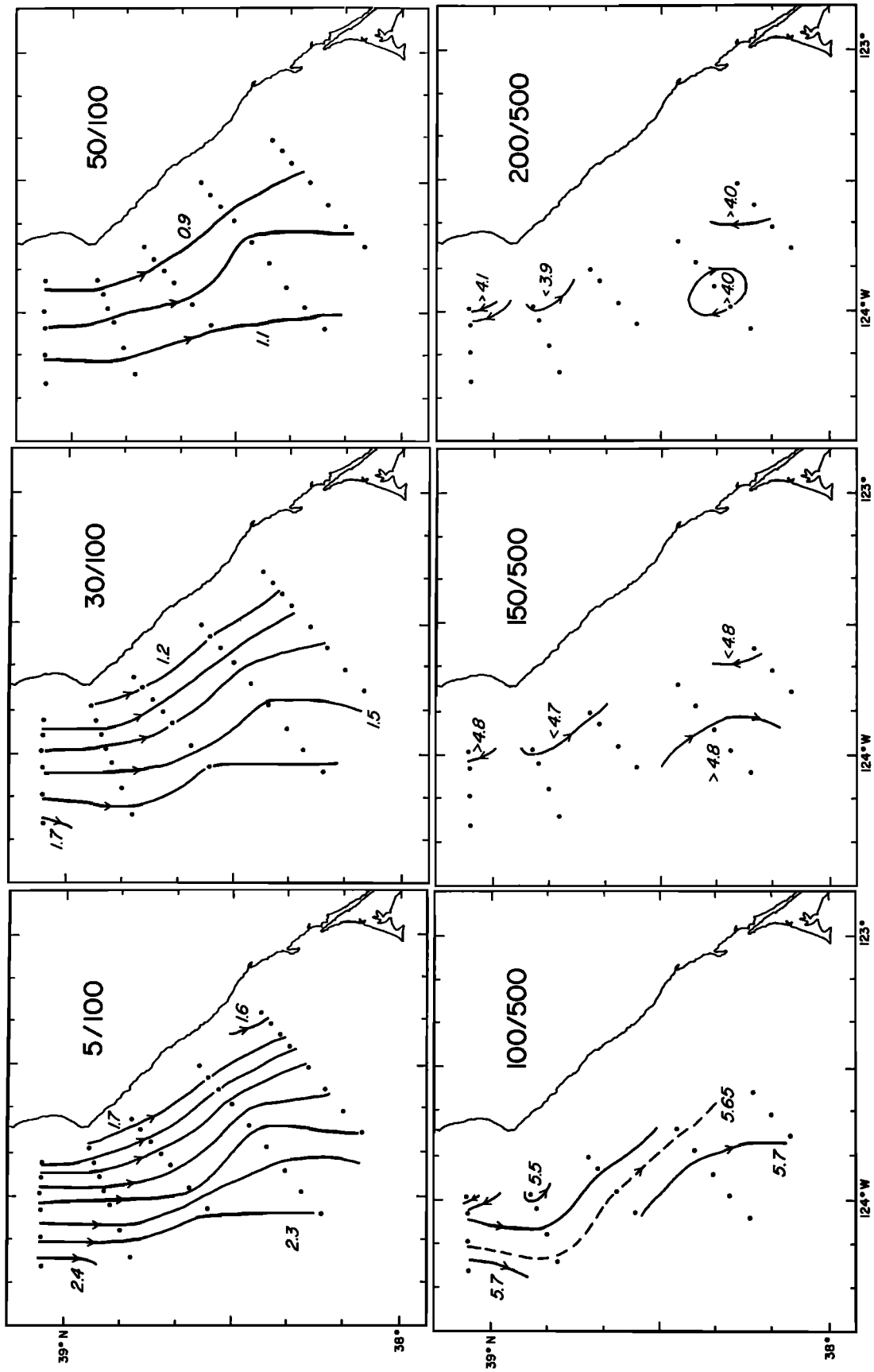

Fig. 21. Overall averages of geopotential anomaly ($m^2 s^{-2}$): (top) at 5, 30, and 50 dbar, relative to 100 dbar, and (bottom) at 100, 150, and 200 dbar, relative to 500 dbar.

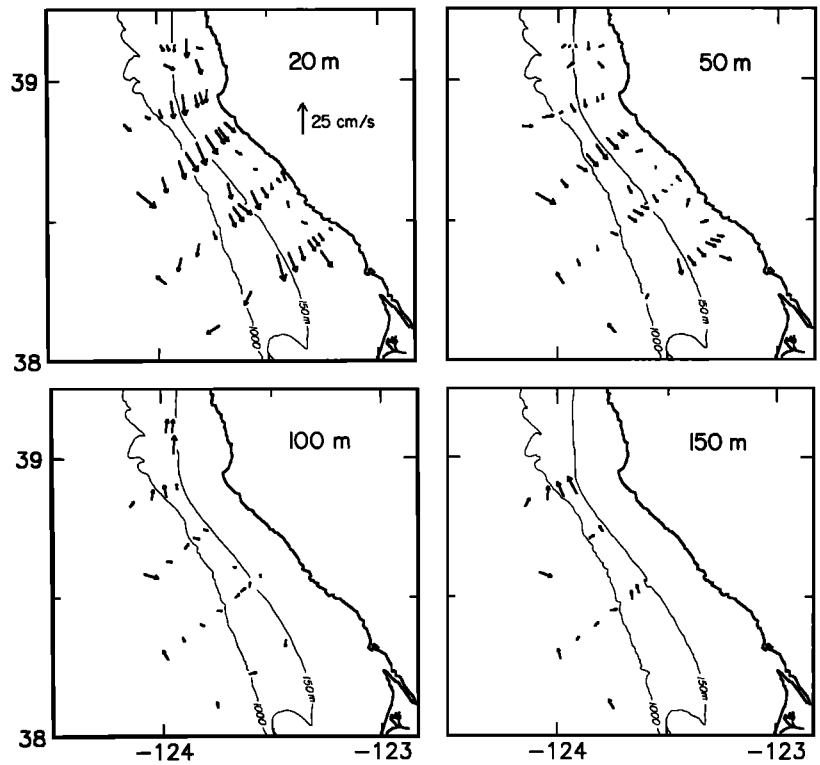

Fig. 22. Overall average of the DAL current vectors at selected depths: 20 m, 50 m, 100 m, and 150 m.

flow decreases from the shelf break to the coast and from north to south (Figure 22); average currents are very weak over the inner shelf in the southern portion of the grid, i.e., at the inshore end of the Central and Ross lines. The weak northward flow at the inshore end of the Central line (Figure 22) is the only signature in the average field of the inshore countercurrent observed so clearly during the April 20–22 and May 29–31 1982, surveys. In the southwestern corner of the grid, beyond the core of the coastal jet, the average 20-m DAL currents are directed offshore. The structure here indicates a clockwise meander or eddy and is consistent with the meander seen in the isohalines and isopycnals at the offshore end of the Central line (compare Figures 19 and 20).

Over the shelf, the average current vectors calculated from the 20-m DAL data (Figure 22) are in good agreement with those estimated (Figure 17) for the near-surface moored current meters when the alongshore wind stress has a value of -1.5 dyn cm^{-2}. (The average wind stress values at NDBO buoy 13 for CODE 1 and CODE 2 are -2.1 and -1.4 dyn cm^{-2}, respectively [*Winant et al.*, this issue]. They are also in good agreement with the average near-surface currents calculated directly from the CODE 2 moored current meter data [*Winant et al.*, this issue, Figure 19*a*]. Average currents at 50 m are very similar to those at 20 m, except that magnitudes are reduced by 30–50%.

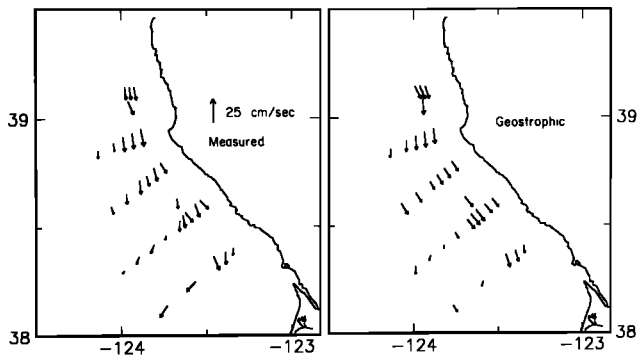

Fig. 23. Distributions of the (left) measured and (right) geostrophic average velocity difference between 20 m and 80 m. Measured velocity differences were calculated directly from the average DAL data; geostrophic velocity differences were calculated by objective mapping of the average geopotential anomalies.

At 100 m, average DAL vectors are generally weak, and no coherent pattern is discernible (Figure 22). The average field at 150 m is rather sparse (DAL profiles did not always extend to this depth), but the available data suggest that there is a narrow (10–20 km) poleward undercurrent adjacent to the continental slope. The poleward current at this depth seems to be both stronger (about 15 cm s^{-1}) and wider (20 km) on the Arena line than on the central line. Its magnitude just seaward of the shelf break on the Central line (6.0 cm s^{-1}) is in reasonable agreement with the CODE 2 mean (5.6 cm s^{-1}) obtained from the 150-m current meter on the C5 mooring over the 500-m isobath [*Winant et al.*, 1985]. This poleward undercurrent is not evident in the average dynamic topography at either 150 m or 200 m (Figure 21). Nor does this directly measured poleward flow explain the northward tending tongue of warm water observed at this depth (Figure 18): the warm tongue lies well seaward of the observed northward flow. We do not know whether this apparent incongruence between the average measured currents, the average geostrophic flow, and the average temperature distribution is due to the limitations (both spatial and temporal) of our sampling scheme or whether it reflects the true state of affairs. One can certainly imagine that the poleward undercurrent may have a strong ageostrophic component and that the temperature dis-

TABLE 2. Inclusive Dates of Synoptic Pairs of Sections Along the Arena and Central Lines, During the Upwelling Season (Mid-April to Mid-August) of 1981 and 1982

Inclusive Times and Dates, UT	Cruise	Station Numbers	
		Arena	Central
CODE 1, 1981			
1956, April 26, to 1906, April 27	leg 4	18–24	32–40
2134, May 2, to 2142, May 3	leg 4	103–108	117–125
1106, May 20, to 1406, May 21	leg 5	43–48	60–68
0948, May 23, to 1904, May 24	leg 5	106–111	95–103
0710, July 8, to 1452, July 9	leg 7	93–98	71–79
0152, July 13, to 2325, July 13	leg 7	136–141	121–129
CODE 2, 1982			
0519, April 21, to 0558, April 22	leg 6	42–47	23–31
1941, May 29, to 2043, May 30	leg 8	100–105	81–89
1741, July 16, to 2120, July 17	leg 9	31–36	14–19
1841, July 19, to 1805, July 21	leg 9	86–91	48–56

tribution may be affected by several processes besides advection by the mean alongshore flow.

5. Comparison of Central and Arena Lines

The average temperature, salinity, and density fields (Figures 18–20) all exhibit a subtle but definite alongshore gradation in at least the upper 100 m. In the maps, this gradient is expressed in the gradual divergence of isopleths from the coastline; each isotherm, isohaline and isopycnal lies nearer shore off Point Arena, where the shelf is narrow, than it does in the southern portion of the grid, where both shelf and slope are wider. On average, near-surface waters off Point Arena appear to be warmer, less saline, and less dense than those farther south. Consequently, the average geopotential anomaly of the sea surface apparently decreases from north to south along the shelf break (Figure 21). Do these apparent average gradients arise because the average fields are contaminated by sampling some lines more frequently than others? Or are they real? If they are real, are they due only to the variation in shelf width; i.e., would they disappear if we used bottom depth rather than offshore distance as a basis for comparison? To answer these questions, we analyzed 10 "synoptic" pairs of Arena and Central line sections; the two sections in each pair were separated by only 1 or 2 days (Table 2). All ten of the pairs were obtained during the upwelling season (between mid-April and mid-August), six in 1981 and four in 1982. From these matched pairs, we calculated pairs of average sections (one each of the Central and Arena lines) for each variable of interest: temperature, salinity, density, and the alongshore component of the measured current. Differences between these averages should be the result of actual spatial gradients and should be free of serious temporal aliasing.

These average sections (Figure 24) indicate that there is a real difference in the average water properties along the Central and Arena lines, which are separated by only about 50 km (Figure 1). At a given distance from shore, surface waters off Point Arena are warmer, less saline, and less dense than those on the Central line. Furthermore, the onshore-offshore gradients of surface water properties are stronger on the Arena line than on the Central line. Differences penetrate to at least the depth of the shelf break: isopleths of all properties rise toward shore more steeply on the Arena line than they do on the Central line. The structure of the variability along the two lines is also different: the variability at the surface is about the same on the two lines, but the salinity and density of deep waters over the midshelf and inner shelf are considerably less variable on the Central line than on the Arena line.

Since we cannot be sure that our 10 pairs represent independent samples, we have not calculated the standard error of the mean but simply show the standard deviations of each variable as a rough measure of the uncertainty. Offshore profiles of surface properties (Figure 25) indicate that the means along the two lines are significantly different at least between 15 and 35 km from shore. In this band, the alongshore difference in each of the surface properties exceeds the standard deviation of that property along either line. We would have liked to calculate the standard deviations of the alongshore differences (since it is clear from the synoptic surveys shown in Figures 3–5 that water properties along the two lines tend to covary), but the strong offshore gradients prevent this: it is not clear a priori which station on the Arena line should be matched to a given station on the Central line. Nevertheless, we conclude that the average alongshore gradation in the surface temperature, salinity, and density fields is a robust feature: within the 40- to 50-km-wide coastal zone, the surface water at a given distance from shore is warmer and less saline on the Arena line than it is on the Central line.

These alongshore gradients do not disappear when we use bottom depth, rather than distance from shore, as the basis for comparison. Figure 26 shows water properties plotted as a function of bottom depth. Note that in this figure the shallow water (the coast) is on the left rather than on the right. Differences between surface water properties on the Arena and Central lines are observed over the entire range of bottom depths; they are largest over the upper continental slope (bottom depths of between 150 and 1000 m). At a depth of 50 m, the mean temperature difference has almost disappeared, but salinity and density differences are still present and are still largest over the continental slope. Significant differences do not penetrate down to the 100-m level.

Averages of the alongshore component of the DAL current along the two lines (Figure 27) were calculated from the same set of 10 matched pairs (Table 2). The DAL data were collected continuously along each line, and averages were calculated at intervals of 2.5 km. The alongshore component was defined to be the component normal to each section, i.e., directed toward 338°T on the Arena line and 320°T on the Central line. Along each line, the average field computed from the 10 matched pairs has the same general structure as does the corresponding overall average described by *Kosro* [this issue, Figure 10].

Average currents along both lines (Figure 27) exhibit the equatorward surface current and strong vertical shear usually associated with the mean onshore density gradient in coastal upwelling regions. Both sections exhibit a poleward undercurrent, which also appears to be an integral feature of most coastal upwelling regimes; the maximum poleward flow is observed just off the shelf break. However, the detailed structure of these features is quite different along the two lines. The equatorward surface current is shallower, weaker, and narrower off Point Arena than on the Central line; its core lies over the inner shelf off Point Arena and over the outer shelf on the Central Line. Off Point Arena, the equatorward surface current spans the entire shelf; on the Central line it is separated from the coast by an inshore countercurrent. The structure of the poleward undercurrent also appears to be different on the two lines: it is considerably stronger and wider off Point

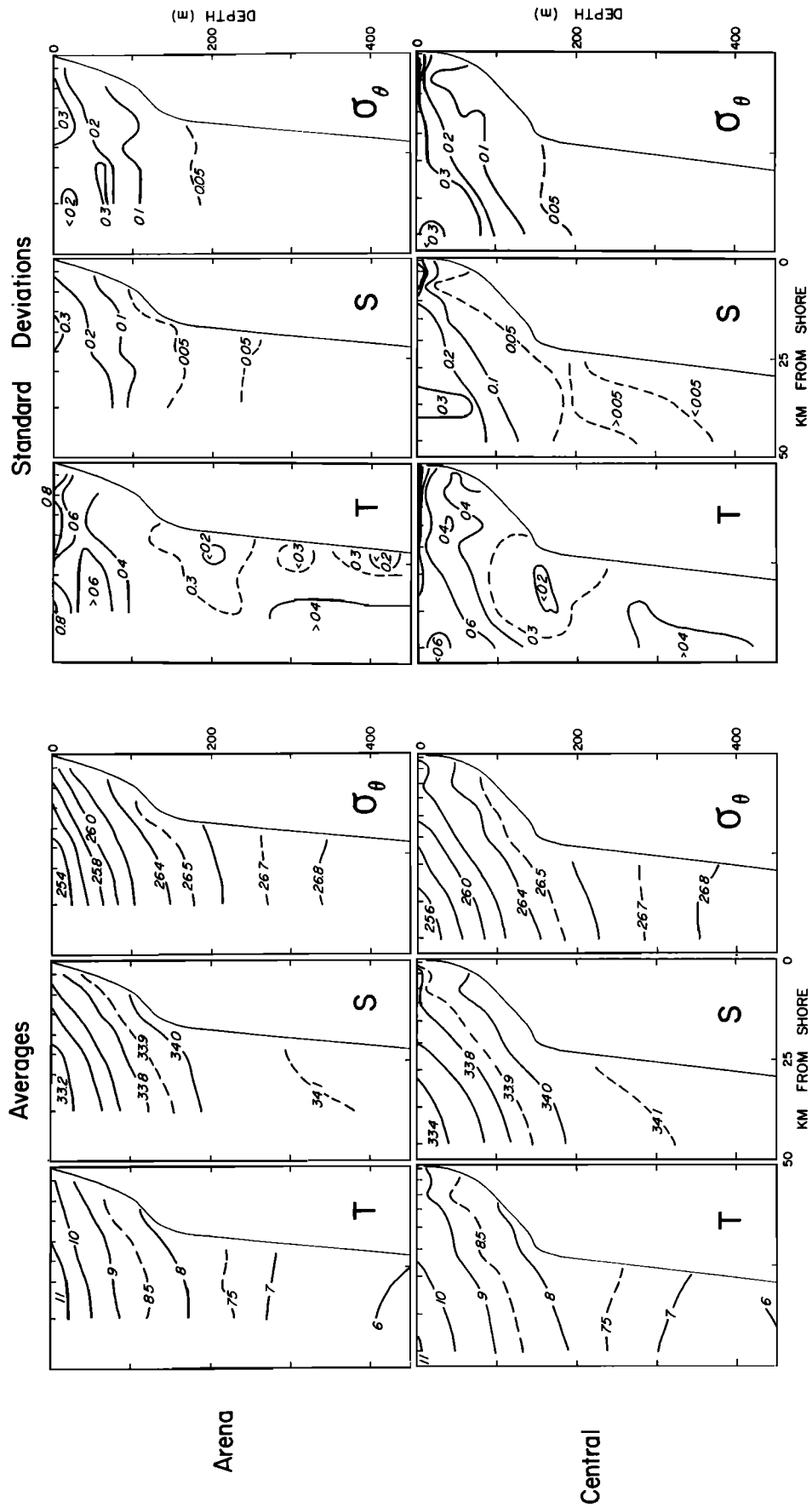

Fig. 24. Vertical sections of the average and standard deviation of temperature, salinity, and density anomaly σ_θ along the Arena and Central lines. These statistics were calculated from the 10 synoptic pairs.

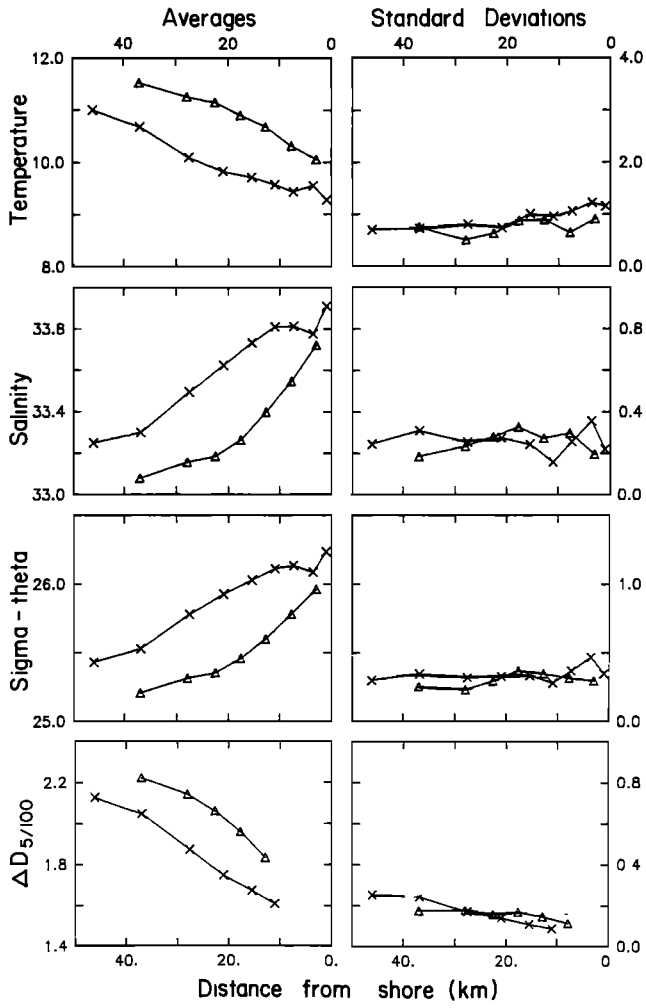

Fig. 25. Offshore profiles of surface (5 m) averages and standard deviations of water properties along the Central (crosses) and Arena (triangles) lines, plotted against offshore distance.

Arena than it is on the Central line. Off Point Arena the undercurrent extends from about midshelf to the offshore end of the section, 37 km from the coast; the line of no motion rises from a depth of 50 m over the inner shelf to a depth of only 10 m offshore. On the Central line the undercurrent seems to be trapped along the bottom: the line of no motion is roughly parallel to the bottom; it deepens from a surface intersection over the inner shelf to a depth of more than 150 m offshore. These differences in the average structure of the undercurrent are intriguing, but they may not be significant; in much of the field, the standard deviation of the alongshore flow is almost as large as (or even larger than) the mean, and only 10 samples are represented.

Are the average alongshore currents in geostrophic balance? This question is difficult to answer directly, since calculating geostrophic velocities in shallow regions with significant bottom slope requires making quite arbitrary assumptions. The method described by *Reid and Mantyla* [1976], for example, assumes that the geostrophic velocity of the water below the greatest common depth of two adjacent CTD stations is the same as the geostrophic velocity between the next offshore pair of stations. This method seems to work quite well for estimating steric height in the CODE region [*Huyer*, 1984]; nevertheless, when we used it to estimate the average geostrophic velocity fields along the Central and Arena lines relative to the 500-dbar level, we obtained patterns quite different from those shown in Figure 27. Given the very narrow (< 10 km) core of the poleward undercurrent and a typical CTD station spacing of 7 km, this disagreement should not be surprising: it is clearly unreasonable to assume that near-bottom velocities very close to the shelf break are the same as those 7 km farther out to sea. It may be possible to develop a technique that works better. Meanwhile, it is useful to compare the geostrophic shear field to the vertical shear of the measured currents.

To obtain the measured current shear, we calculated the differences between average DAL current data at successive depths and divided this difference by the vertical separation (6.5 m); adjacent DAL profiles ae 2.5 km apart. To reduce noise levels, these estimates were smoothed both vertically and horizontally with a triangular filter. Geostrophic shear estimates were obtained in the same way: they have the same vertical resolution but variable (and much coarser) horizontal resolution. Gross features of the geostrophic and measured shear fields (Figure 28) are similar. Both are negative throughout most of the water column above 150 m. On both lines, strongest shears (measured and geostrophic) are observed at the surface: over the inner shelf off Point Arena, and over the outer shelf on the Central line. On the Arena line a high-shear zone extends downward from the surface over the inner shelf to a depth of 50–70 m offshore. In the 30- to 80-m depth range, both measured and geostrophic shears are stronger off Point Arena than on the Central line. These gross similarities indicate that at least to a good first approximation, the alongshore velocity within most of the upper 150 m is geostrophic.

In one respect, the measured and geostrophic shear fields are quite different: strongest measured shears, which occur within the upper 30–40 m, are about twice as large as the strongest geostrophic shears (Figure 28). On the Arena line, where this high-shear zone is quite narrow, this difference may be the result of the relatively coarse (5 km) CTD station spacing. On the Central line, however, the high-shear zone is sufficiently wide (15 km) to be resolved by our CTD stations; even here, the shear calculated from the DAL data is much larger than the average geostrophic shear. The moored current meter data [*Winant et al.*, this issue] also show very strong average shear ($4–5 \times 10^{-3}$ s^{-1}) in the upper 35 m over the outer shelf on the Central line. Thus at least on the Central line, there appears to be a significant mean ageostrophic shear which decreases from 2.5×10^{-3} s^{-1} at 15 m (our shallowest DAL bin) to less than 1.0×10^{-3} s^{-1} at depths below 40 m. This mean ageostrophic shear may be driven by the large mean alongshore wind stress. If we assume simple Ekman dynamics with a constant eddy viscosity A_z and an Ekman depth $D_E = (2A_z/f)^{1/2}$ of 20 m, we can calculate the onshore and alongshore components of the Ekman (ageostrophic) velocity as a function of depth, and hence the theoretical ageostrophic shear. Assuming a steady alongshore wind stress of -1.5 dyn cm^2, we find that the alongshore component of the shear associated with the Ekman spiral falls from -2.9×10^{-3} s^{-1} at 15 m to zero at 31 m, in general agreement with the observed difference between the measured and geostrophic shear fields of Figure 28.

6. Discussion and Conclusions

The mesoscale CTD and velocity surveys conducted over the continental shelf and slope as part of the Coastal Ocean

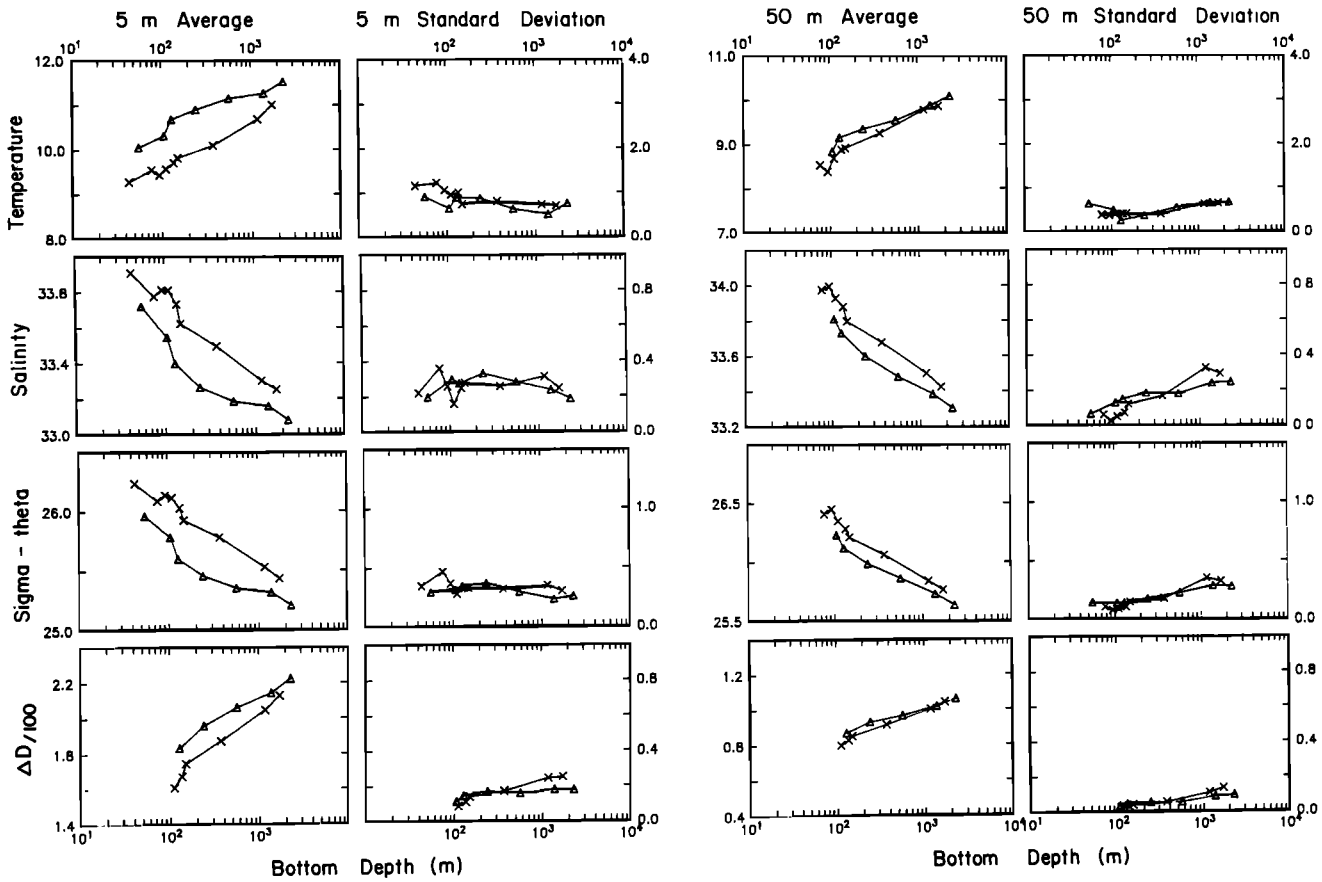

Fig 26 Offshore profiles of water properties along the Central (crosses) and Arena (triangles) lines, plotted against bottom depth, for properties at depths of 5 m and 50 m.

Dynamics Experiment have provided a wealth of information on the structure and variability of the coastal zone near Point Arena. All of our synoptic surveys were made between April and August, when the seasonal wind is predominantly favorable for upwelling. Three of the surveys were made during strong upwelling events (winds exceeding 20 knots or 10 m s^{-1}), and three were made during "relaxations", i.e., periods when the usually strong upwelling-favorable winds had weakened or even reversed. As was expected, surface water properties reflected the weather. Surface temperatures increased (and

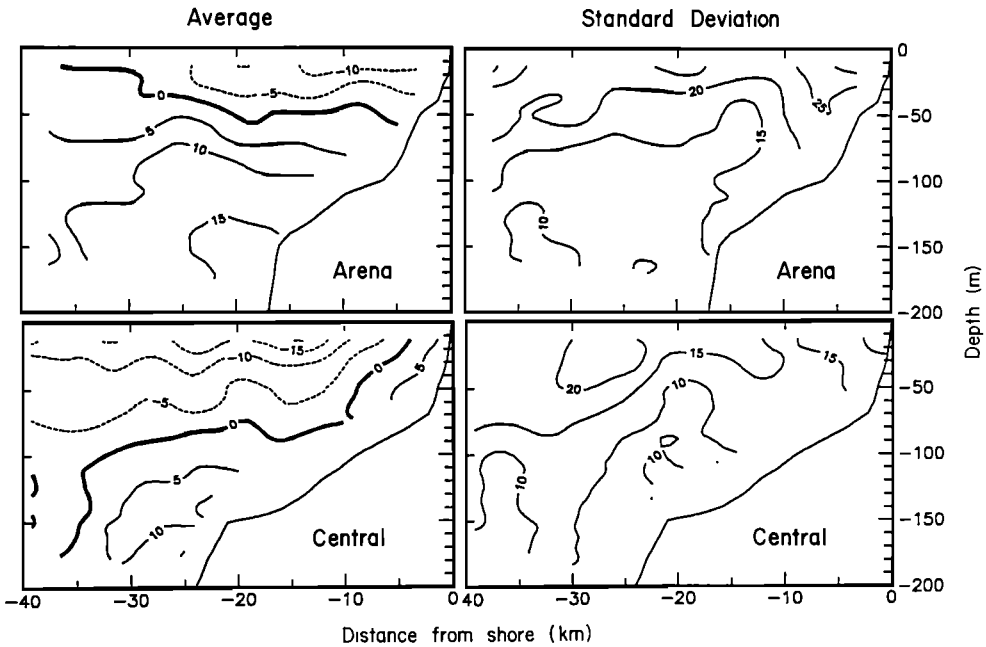

Fig. 27. Vertical sections of the (left) average and (right) standard deviation of the alongshore component of the velocity (in centimeters per second) along (top) the Arena line and (bottom) the Central line The alongshore component was defined to be directed toward 338°T on the Arena line and 320°T on the Central line.

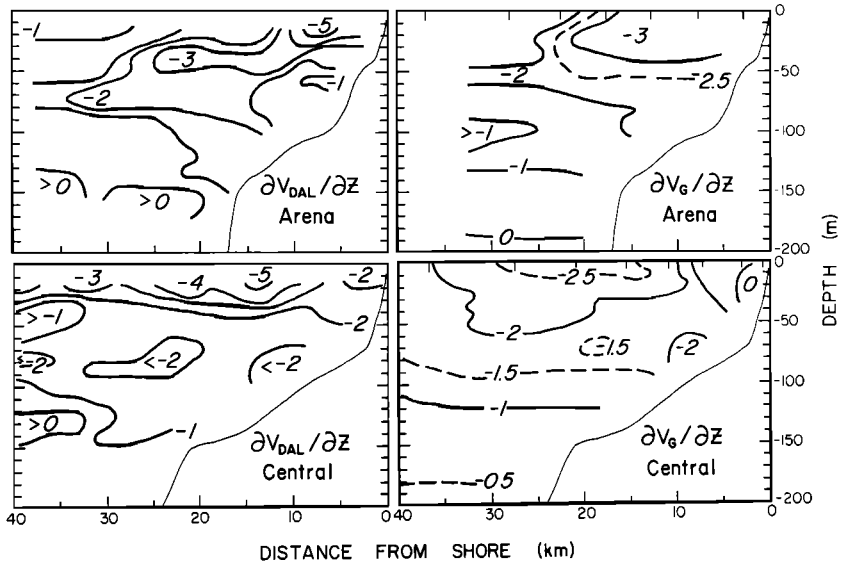

Fig. 28. Vertical sections of (left) the measured shear ($\partial V_{DAL}/\partial z$) calculated from the average DAL data and (right) the geostrophic shear ($\partial V_G/\partial z$) calculated from the average density sections along (top) the Arena line and (bottom) the Central line. Units are 10^{-3} s^{-1}.

salinities decreased) monotonically with distance from shore during the three windy surveys. Surface temperature and salinity distributions were more complex when winds were weak. The surface temperature fields also reflect the influence of surface heating: the temperature difference between the surface and 20 m was only 0.5°–1.0°C when winds were strong but as large as 2°C when winds were weak.

The surface salinity field is influenced by alongshore advection as well as by the direct effects of coastal upwelling. A pool of low-salinity water of more northern origins seems to recur or persist just off Point Arena; it sometimes coincides with an anticyclonic eddy or meander and may be associated with the formation of strong, narrow currents directed out to sea which are referred to as "squirts" or "seaward jets" [*Davis*, 1985*a*; *Kosro and Huyer*, 1986]. Low surface salinities were observed inshore during the two surveys in the spring of 1982 when local runoff (through the Russian River and San Francisco Bay) was very high; the low-salinity water was advected northward along the coast by a narrow inshore countercurrent that seems to recur whenever winds are weak.

The circulation patterns observed during all but one of the synoptic surveys were much more complicated than we had expected. These complex patterns are coherent over scales of 10–100 km, and they are associated with definite features in the corresponding satellite infrared images [*Kosro*, 1986]; they are not the result of aliasing tidal and inertial signals or other sources of noise. Previous studies of coastal upwelling in regions with simpler topography had indicated that alongshore gradients were generally much weaker than onshore-offshore gradients, particularly during strong winds (see, for example, Figure 14 of *Brink* [1983]). A baroclinic alongshore coastal jet with strongest equatorward velocities at the surface over the midshelf or outer shelf and a poleward undercurrent over the shelf break or upper slope appeared to be integral features of the upwelling regime [*Huyer*, 1983; *Brink et al.*, 1983; *Mittelstaedt*, 1983]. Previous studies had also indicated that the ratio of the alongshore component of the current to the onshore component was considerably larger during strong upwelling events than during weak winds, i.e., that upwelling circulation patterns are more nearly two-dimensional when winds are strong [*Halpern*, 1976; *Smith*, 1981]. This classical two-dimensional flow pattern was observed during one of our surveys, in April 1982. Its absence in the other five surveys cannot be attributed to the concurrent winds (three had strong winds, while two had weak or variable winds). Its presence in April 1982 may be associated with a large-scale seasonal cycle: each year in late winter or early spring there is a rapid spring transition which marks the onset of a persistent equatorward surface current [*Strub et al.*, this issue]; the southward current seems to persist over the shelf for a few months off northern Oregon and Washington but for only a few weeks off central California [*Strub et al.*, this issue]. In 1982 the spring transition event occurred in mid-April [*Lentz*, this issue], only a week before the April 20–22 survey with the classical two-dimensional coastal jet. In 1981 the spring transition occurred in late March [*Lentz*, this issue], a full month before our first survey; data from the SuperCODE project (which included a large-scaled moored array over the shelf from 35°N to 48°N) indicated that strong southward currents persisted at 42°N from March 25 to at least April 10 [*Strub et al.*, this issue], and data from the CODE 1 moored array [*Mills and Beardsley*, 1983] suggest that a strong southward current was present in the CODE region until April 15.

How and why this simple two-dimensional flow pattern breaks down is not clear. The remaining five surveys suggest that a baroclinic equatorward jet is still present, but with bifurcations and meanders: it can wind between eddies and even turn directly offshore. A particular mesoscale pattern persists for at least several days [*Kosro*, this issue] but not for the several-week interval that typically separates our surveys. One possible mechanism for the formation of these mesoscale meanders and eddies involves the quasi-barotropic inshore countercurrent and the bend in the coastline at Point Arena. Consider a simple, southward barotropic current over the shelf: as it flows past Point Arena, its southward momentum will cause it to cross isobaths; to conserve potential vorticity, it will tend to turn left, i.e., back toward its original isobath, and continue flowing along the coast. Now consider a simple northwestward barotropic current: as it flows past Point Arena, it too will tend to cross isobaths and turn left to con-

serve potential vorticity; this, however will take it into still deeper water and cause the relative vorticity to increase still further. Although this conceptual model is too simple to fully represent the dynamics of the (largely baroclinic) flow field in the CODE region, it does suggest that eddies or meanders would develop off Point Arena whenever an inshore poleward countercurrent is present; data from the CODE moored array indicate that this occurs whenever the upwelling-favorable wind relaxes, i.e., two or three times a month.

The complex mesoscale structures seen in the synoptic surveys are not present in our overall average fields nor in the average surface current field computed from the very complex CODE drifter tracks [*Davis*, 1985*a*, *b*]. Neither are they seen in the averages calculated from the current meter array moored over the shelf [*Winant et al.*, this issue]. The eddies and meanders generally seem to average out, though there is some evidence of an average meander in the southwest portion of the survey grid. The average flow pattern has a definite baroclinic equatorward surface current with a weak maximum over the upper continental slope, a very weak inshore countercurrent, and a definite undercurrent at the shelf break. The average temperature, salinity, and density fields are congruent with this flow pattern: all have the strong onshore-offshore gradients typical of coastal upwelling regimes. The onshore density gradient implies that the shear of the alongshore flow is negative from the surface to at least 200 m. In the surface layers, the average isotherms, isohalines, and geostrophic streamlines all diverge from the coast: they are nearer shore off Point Arena than farther south. This divergence is also seen in the average surface temperature field calculated from satellite infrared imagery [*Kelly*, 1985]. The divergence does not seem to be the result of isotherms, etc., turning to the right, away from the coast; rather, the coastline bends sharply to the left away from the relatively straight isopleths.

The comparison of averages of 10 matched pairs of Central and Arena line sections confirms that there is a systematic difference between them. Warmer, fresher waters lie nearer shore off Point Arena than on the Central line. Each surface isotherm and isohaline actually lies in shallower water on the Arena line than it does on the Central line. This observation lends support to the idea that the momentum of an alongshore current (in this case the equatorward surface flow) may cause it to cross isobaths. Comparison of the average currents on the two lines indicates there are also systematic differences in the vertical structure of the poleward undercurrent: on the Central line it seems to be trapped along the continental margin, and on the Arena line it seems to be leaving the margin. While those would be consistent with the simple potential vorticity argument discussed above, we must point out that this difference may be more apparent than real: the standard deviations of the flow at this depth are roughly the same size as the means.

While our mesoscale surveys have provided a great deal of information and some new insights into the structure and variability of a coastal upwelling regime, they also raise interesting questions for further investigation. We hope that future experiments will shed more light on the structure and dynamics of the poleward undercurrent and on the formation of eddies, meanders, and squirts in the coastal zone.

Acknowledgments. We are grateful to all those who participated in the planning, execution and analysis of the CODE mesoscale surveys: our colleagues in CODE, the crew of the R/V *Wecoma*, and all those who stood hydro watches on the CODE cruises. We especially thank Russ Davis and Lloyd Regier for sponsoring the CODE DAL component and Rich Schramm and Jane Fleischbein for assisting in the analysis of the CTD data. We have benefitted a great deal from discussions with Russ Davis, Bob Smith, Dudley Chelton, John Allen, and Steve Lentz. The observations and analysis presented here were funded by the National Science Foundation (grants OCE-8014943 and OCE-8410861 to Oregon State University and grants OCE-8014942 and OCE-8410546 to Scripps Institution of Oceanography) and by the Office of Naval Research (contract N00014-80-C0440 to Scripps Institution of Oceanography).

REFERENCES

Beardsley, R. C., and C. A. Alessi, CODE-2: An array description of the surface wind and near-surface currents, CODE-2 Moored Array and Large-Scale Data Report, edited by R. Limeburner, *CODE Tech. Rep. 38*, *WHOI Tech. Rep. 85-35*, pp. 109–131, Woods Hole Oceanogr. Inst., Woods Hole, Mass., 1985.

Beardsley, R. C., R. C. Limeburner, and L. K. Rosenfeld, Introduction to the CODE-2 moored array and large-scale data report,: CODE-2 Moored Array and Large-Scale Data Report, edited by R. Limeburner, *CODE Tech. Rep. 38*, *WHOI Tech. Rep. 85-35*, pp. 1–21, Woods Hole Oceanogr. Inst., Woods Hole, Mass., 1985.

Bretherton, F. P., R. E. Davis, and C. B Fandry, A technique for analysis and design of oceanography experiments applied to MODE-73, *Deep Sea Res.*, *23*, 559–582, 1976.

Brink, K. H., The near-surface dynamics of coastal upwelling, *Prog. Oceanogr.*, *12*, 223–257, 1983.

Brink, K. H., D. Halpern, A. Huyer, and R. L. Smith, The physical environment of the Peruvian upwelling system, *Prog. Oceanogr.*, *12*, 285–305, 1983.

Davis, R. E., Current-following drifters in CODE, *CODE Tech. Rep. 10*, *SIO Ref. 83-4*, 44 pp., Scripps Inst. of Oceanogr., La Jolla, Calif., 1983.

Davis, R. E., Drifter observations of coastal surface currents during CODE: The method and descriptive view, *J. Geophys. Res.*, *90*, 4741–4755, 1985*a*.

Davis, R. E., Drifter observations of coastal surface currents during CODE. The statistical and dynamical views, *J. Geophys. Res.*, *90*, 4756–4772, 1985*b*

Fleischbein, J., W. E. Gilbert, and A. Huyer, Hydrographic data from the First Coastal Ocean Dynamics Experiment: Leg 4, 25 April–7 May 1981, *CODE Tech. Rep. 5*, *Data Rep. 92*, *Ref. 82-2*, 149 pp., School of Oceanogr., Oreg. State Univ., Corvallis, 1982.

Fleischbein, J., W. E. Gilbert, and A. Huyer, Hydrographic Data from the Second Coastal Ocean Dynamics Experiment: R/V *Wecoma*, Leg 6, 18–24 April 1982, *CODE Tech Rep. 11*, *Data Rep. 102*, *Ref. 83-4*, 86 pp., School of Oceanogr., Oreg. State Univ., Corvallis, 1983*a*.

Fleischbein, J., W. E. Gilbert, and A. Huyer, CTD Observations off Oregon and California· R/V *Wecoma*, W8205A and *CODE* 2 leg 8, 18 May–4 June 1982, *CODE Tech. Rep. 16*, *Date Rep. 104*, *Ref. 83-10*, 149 pp., School of Oceanogr., Oreg. State Univ., Corvallis, 1983*b*.

Gilbert, W. E., J. Fleischbein, A. Huyer, and R. Schramm, Hydrographic Data from the First Coastal Ocean Dynamics Experiment: R/V *Wecoma*, Leg 5, 16–29 May 1981, *CODE Tech. Rep. 6*, *Data Rep. 93*, *Ref. 82-5*, 178 pp., School of Oceanogr., Oreg. State Univ., Corvallis, 1982.

Halliwell, G. R., Jr., and J. S. Allen, CODE-1· Large-scale wind and sea level observations, CODE-1 Moored Array and Large-Scale Data Report, edited by L. K. Rosenfeld, *WHOI Tech. Rep. 83-23*, pp. 131–185, Woods Hole Oceanogr. Inst., Woods Hole, Mass., 1983

Halliwell, G R., Jr., and J. S. Allen, CODE-2: Large-scale wind and sea level observations, CODE-2: Moored Array and Large-Scale Data Report, edited by R. Limeburner, *CODE Tech. Rep. 38*, *WHOI Tech. Rep. 85-35*, pp. 179–233, Woods Hole Oceanogr. Inst., Woods Hole, Mass., 1985.

Halpern, D., Structure of a coastal upwelling event observed off Oregon during July 1973, *Deep Sea Res.*, *23*, 495–508, 1976.

Huyer, A., Coastal upwelling in the California current system, *Prog. Oceanogr.*, *12*, 259–284, 1983.

Huyer, A., Hydrographic observations along the CODE central line off northern California, 1981, *J. Phys. Oceanogr.*, *14*, 1647–1658, 1984.

Huyer, A., J. Fleischbein, and R. Schramm, Hydrographic data from

the Second Coastal Dynamics Experiment: R/V *Wecoma*, Leg 9, 6–27 July 1982, *Data Rep. 109*, *Ref. 84-7*, 130 pp., School of Oceanogr. Oreg. State Univ., Corvallis, 1984.

Kelly, K. A., The influence of winds and topography on the sea surface temperature patterns over the northern California slope, *J. Geophys. Res.*, *90*, 11,783–11,798, 1985.

Kosro, P. M., Shipboard acoustic current profiling during the Coastal Ocean Dynamics Experiment, *SIO Ref. 85-8*, 119 pp., Scripps Inst. of Oceanogr., La Jolla, Calif., 1985.

Kosro, P. M., Structure of the coastal current field off northern California during the Coastal Ocean Dynamics Experiment, *J. Geophys. Res.*, this issue.

Kosro, P. M , and A. Huyer, CTD and velocity surveys of seaward jets off northern California, July 1981 and 1982, *J. Geophys. Res.*, *91*, 7680–7690, 1986.

Kundu, P. K., and J. S. Allen, Some three-dimensional characteristics of low-frequency fluctuations near the Oregon coast, *J. Phys. Oceanogr.*, *6*, 181–199, 1976.

Lentz, S. J., A description of the 1981 and 1982 spring transitions over the northern California shelf, *J. Geophys. Res.*, this issue.

Markham, K. L., V. Piro, W. F. Shelton, and M. W. Weston, Jr., Water resources data, California, Water year 1982, vol. 2, Pacific slope basins from Arroyo Grande to Oregon state line except Central Valley, *Rep. USGS/WRD/AD-84-020*, p. 220, Water Resour. Div., U.S. Geol. Surv., Sacramento, Calif., 1984.

Mills, C. A., and R. C. Beardsley, CODE-1: Coastal and moored meteorological observations, CODE-1: Moored Array and Large-Scale Data Report, edited by L. K. Rosenfeld, *WHOI Tech. Rep. 83-23*, pp. 17–53, Woods Hole Oceanogr. Inst., Woods Hole, Mass., 1983.

Mittelstaedt, E., The upwelling area off northwest Africa—A description of phenomena related to coastal upwelling, *Prog. Oceanogr.*, *12*, 307–331, 1983.

Nelson, C. S., and D. M. Husby, Climatology of Surface Heat Fluxes over the California Current Region., *NOAA Tech Rep., NMFS-SSRF-763*, 155 pp., 1983.

Olivera, M., W. E. Gilbert, J. Fleischbein, A. Huyer and R. Schramm, Hydrographic data from the First Coastal Ocean Dynamics Experiment: R/V *Wecoma*, Leg 7, 1–14 July 1981, *CODE Tech. Rep. 7*, *Data Rep. 95*, *Ref. 82-8*, 163 pp., School of Oceanogr., Oreg. State Univ., Corvallis, 1982.

Reid, J. L., and A. W. Mantyla, The effect of geostrophic flow upon coastal sea elevations in the northern North Pacific Ocean, *J. Geophys. Res.*, *81*, 3100–3110, 1976.

Reid, J. L., Jr., G. I. Roden, and J. G. Wyllie, Studies of the California Current System, progress report, 1 July 1956–1 Jan. 1958, pp. 28–56, Calif. Coop. Fish. Invest., La Jolla, 1958.

Smith, R. L., A comparison of the structure and variability of the flow field in the three coastal upwelling regions: Oregon, northwest Africa, and Peru, in *Coastal Upwelling, Coastal and Estuarine Sci.*, vol. 1, edited by F. A. Richards, pp. 107–118, AGU, Washington, D. C., 1981.

Strub, P. T., J. S. Allen, A. Huyer and R. L. Smith, Large-scale structure of the spring transition in the coastal ocean off western North America, *J. Geophys. Res.*, this issue.

U. S. Geological Survey, Water resources data, California, Water year 1981, vol. 2, Pacific slope basins from Arroyo Grande to Oregon state line except Central Valley, *Water Data Rep. CA-81-2*, p. 267, Sacramento, Calif., 1981.

Winant, C. D., U. Send, and S. J. Lentz, CODE-2 moored current observations, CODE-2: Moored Array and Large-Scale Data Report, edited by R. Limeburner, *CODE Tech. Rep. 38*, *WHOI Tech. Rep. 85-35*, pp. 73–107, Woods Hole Oceanogr. Inst., Woods Hole, Mass., 1985.

Winant, C. D., R. C. Beardsley, and R. E. Davis, Moored wind, temperature, and current observations made during Coastal Ocean Dynamics Experiments 1 and 2 over the northern California continental shelf and upper slope, *J. Geophys. Res.*, this issue.

A. Huyer and P. M. Kosro, College of Oceanography, Oregon State University, Corvallis, OR 97331.

(Received May 19, 1986;
accepted June 11, 1986.)